SAND80-1583
Unlimited Release
UC-62

Analytical Studies of a Parabolic Line Concentrator Utilizing an Aluminum Honeycomb Support Structure and a Thin Glass Reflector Laminate

J. Richard Koteras

Prepared by Sandia National Laboratories, Albuquerque, New Mexico 87185 and Livermore, California 94550 for the United States Department of Energy under Contract DE-AC04-76DP00789

Printed March 1981

Sandia National Laboratories

TOTAL PAGES: 84

Includes all paginated and Non-Paginated Pages.

Printed in the United States
of America

Available from
National Technical Information
Service
U.S. Department of Commerce
5285 Port Royal Road
Springfield, VA 22161

Price: Printed Copy $8.00;
Microfiche A05

SAND80-1583
Unlimited Release
Distribution Category UC-62

ANALYTICAL STUDIES OF A PARABOLIC LINE CONCENTRATOR UTILIZING AN ALUMINUM HONEYCOMB SUPPORT STRUCTURE AND A THIN GLASS REFLECTOR LAMINATE*

J. Richard Koteras
Division 5523
Sandia National Laboratories**
Albuquerque, NM 87185

Abstract

Results (stresses, displacements, and equivalent slope errors) are presented from finite element analyses made to evaluate a design for a parabolic trough solar concentrator. The concentrator consists of a reflector laminate (made of thin glass bonded to sheet metal backing) which is mechanically formed and bonded to a stiff parabolic support (made of aluminum honeycomb bonded to steel skins) with a 2 meter (6.6 foot) aperture. Analyses were first made to determine a length for the concentrator such that it would meet certain performance and survivability criteria under wind and gravity loadings. These studies were made with a model for the concentrator only. The concentrator model was then combined with a model for a support mechanism, and this combined structure was studied for several wind and gravity loadings. A design characterized by a six meter (twenty foot) long concentrator was found to meet performance criteria and had sufficiently low glass stresses in a 40.23 meter per second (ninety mile per hour) wind.

---

* This work was supported by the U. S. Department of Energy Contract DE-AC094-76DP00789

** A U. S. Department of Energy Facility

ACKNOWLEDGEMENTS

The author wishes to thank S. B. Martin, R. C. Reuter, Jr., and S. Thundborg, Jr., for their assistance during the analysis phase of this project. The comments and suggestions from S. B. Martin, R. T. Othmer, and R. C. Reuter, Jr., regarding the initial draft of this report are greatly appreciated.

TABLE OF CONTENTS

INTRODUCTION

The following report discusses structural studies for a parabolic trough solar concentrator. The concentrator consists of a reflector laminate bonded to a stiff support structure. The reflector laminate consists of thin (on the order of 0.254 mm (0.01 in) to 0.508 mm (0.02 in) silvered glass bonded to a sheet metal backing. The studies were made to determine a reflector laminate-support combination which met certain structural and optical criteria. All of the computer results presented for the various studies discussed in this report are from the structural analysis code NASTRAN [1].

CONCENTRATOR DIMENSIONS

The trough under study has a parabolic cross-section with a ninety-two degree rim angle and a two meter aperture. The values for various cross-section parameters are shown in Figure 1. The length of the concentrator is one of the dimensions which varies in the studies that are presented. It is desirable to have a long concentrator so as to minimize the number of supports and drive mechanisms required for an entire collector system. The length of a concentrator is limited by the fact that one wants to avoid a "thick" support so as to minimize the weight per unit area and, in some instances, simplify fabrication, handling, shipping, and installation.

Laminates for the concentrator are shown in Figure 2. One laminate has glass which is 0.254 mm (0.01 in) thick, and the

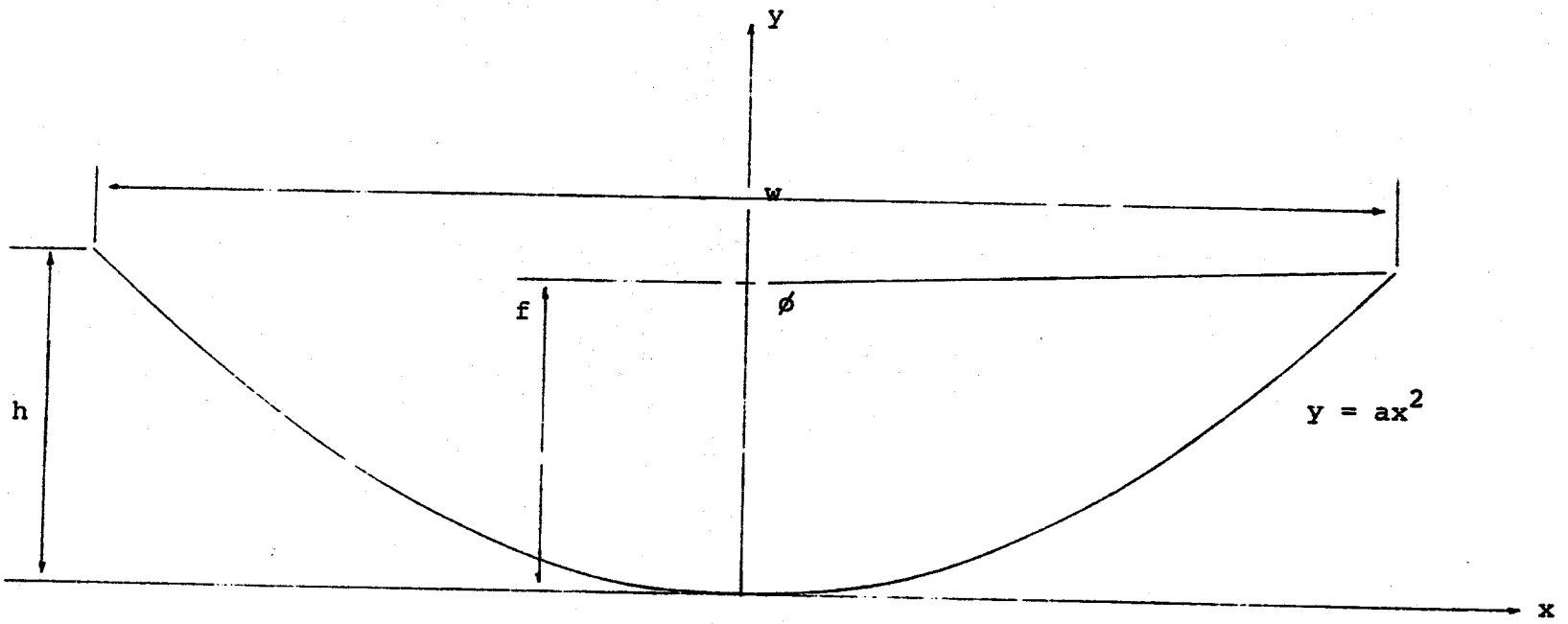

ø = rim angle = 92°
w = aperture width = 2 m
f = focal length = 0.428 m
h = height = 0.5178 m
a = 0.5178 1/m (from $y = ax^2$)

Figure 1. Parameters for Cross-Section of Parabolic Reflector

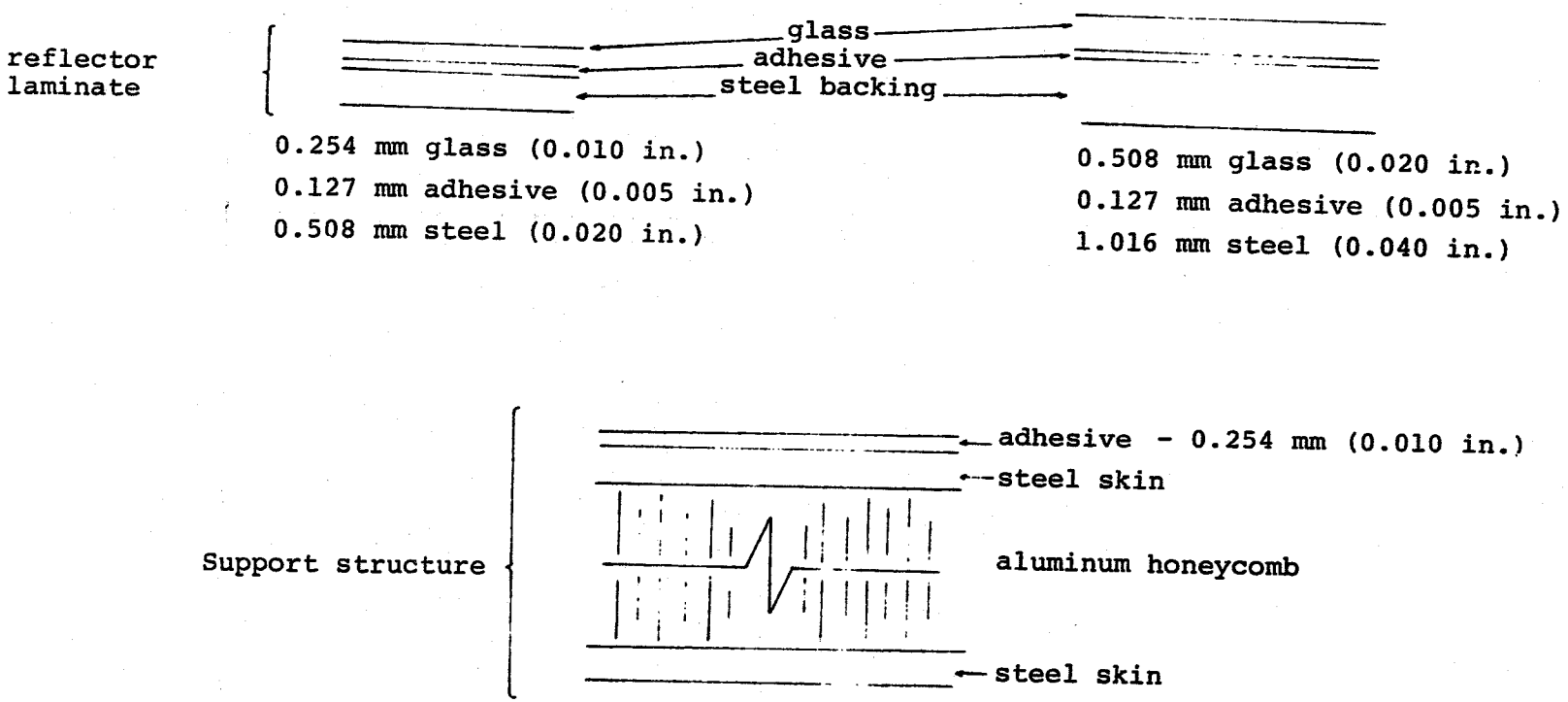

Figure 2. Reflector Laminates and Support for Parabolic Reflector

other laminate has glass which is 0.508 mm (0.02 in) thick. The laminate is bonded to the support by a 0.254 mm (0.01 in) thick layer of adhesive. The support structure consists of an aluminum honeycomb core bonded to steel skins.

PRELIMINARY STUDIES

There were some preliminary studies done not only to determine a possible length for the concentrator, but also the construction of the support structure, i.e., core and skin thickness. These initial studies were done with a finite element model of the concentrator consisting solely of plate elements. This model is shown in Figure 3. The view in Figure 3 shows the mesh for the concentrator in a flattened shape. The global coordinate system for the concentrator is shown in Figure 4. All loading conditions which are discussed for the preliminary studies are symmetric about the cross-sectional plane cutting the trough midway along its longitudinal axis. Because of this, only half the concentrator is modeled. The trough is simply supported at three points that cannot move vertically (in the +Y direction), but they are free to move in and out of the X-Y plane.

The first model studied was a three meter long trough. The support structure consisted of 0.0381 m (1.5 in) thick aluminum honeycomb covered by 0.3302 mm (0.013 in) thick steel skins. This support structure combined with a laminate made of 0.508 mm (0.02 in) glass bonded to a 1.016 mm (0.04 in)

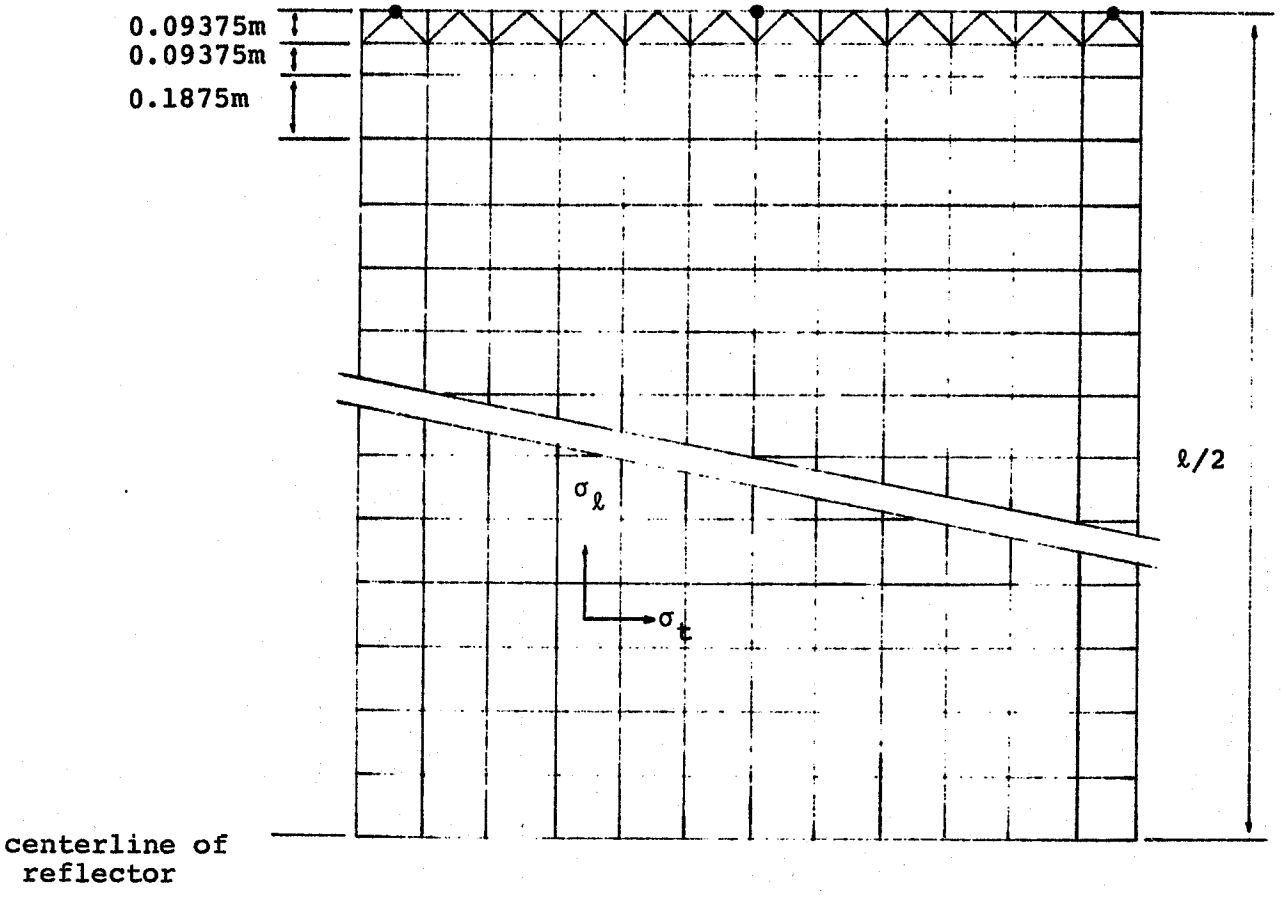

Figure 3. Finite Element Mesh for Initial Structural Studies

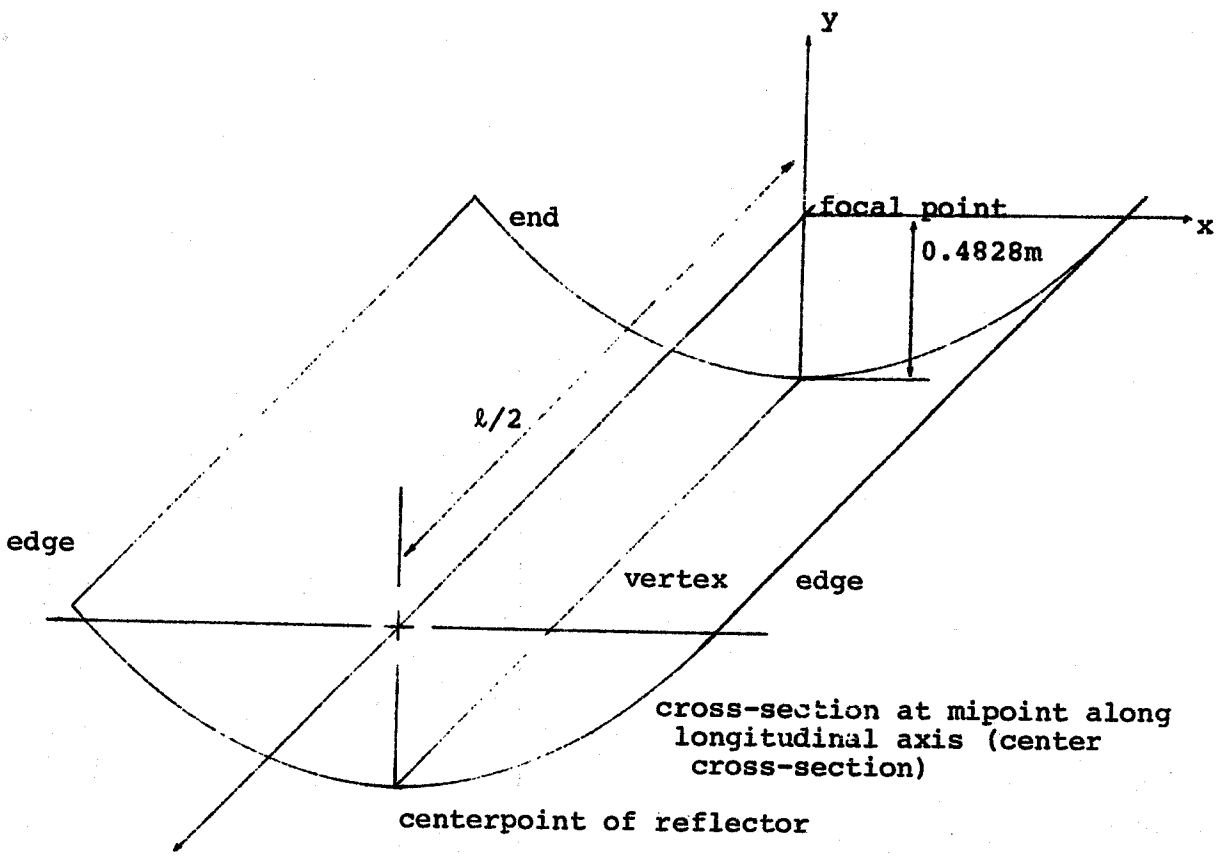

x, y, z is global coordinate system

Figure 4. Global Coordinate System for Mesh Shown in Figure 3

Table 1.

Deflections for 3.0 Meter Long Reflector: support - 0.0381 m honeycomb, 0.3302 mm steel 0.3302 mm steel skins; laminate - 0.508 mm glass, 1.016 steel backing; gravity acting in -y direction.

Global Coordinates			Deflections		
x meters	y meters	z meters	u_x meters	u_y meters	θ_z radians
-1.0000	0.0349	1.5000	9.9046×10^{-6}	-9.1146×10^{-6}	-3.9446×10^{-5}
-0.8611	-0.0989	1.5000	4.9616×10^{-6}	-1.4388×10^{-5}	-3.3549×10^{-5}
-0.7116	-0.2207	1.5000	1.6648×10^{-6}	-1.8532×10^{-5}	-2.0956×10^{-5}
-0.5502	-0.3261	1.5000	1.9015×10^{-7}	-2.0857×10^{-5}	-7.9991×10^{-5}
-0.3765	-0.4095	1.5000	-8.5262×10^{-8}	-2.1472×10^{-5}	2.0114×10^{-7}
-0.1916	-0.4638	1.5000	-4.3750×10^{-9}	-2.1186×10^{-5}	2.1660×10^{-6}
0.0	-0.4828	1.5000	0.0	-2.0951×10^{-5}	0.0

steel backing was subjected to gravity loading (gravity acting in the -Y direction in Figure 4). For this particular construction and loading configuration, the deflections along the center cross-section were extremely small. The deflections for the center cross-section are listed in Table 1.

Because of these small deflections, it was decided that longer concentrator lengths and thinner honeycomb sections should be considered. Additional studies revealed that concentrator lengths greater than or equal to 4.875 m (sixteen ft) and a honeycomb thickness of 0.0254 m (1.0 in) should be considered in future analyses. The analyses leading to these conclusions were based on the mesh shown in Figure 3. A number of approximations in the model shown in Figure 3 resulted in a structural representation which was too stiff, although not by a large amount. This model was sufficiently accurate for the determination of the construction of the support. It was also good enough to give an estimate for a reasonable concentrator length corresponding to some given support cross-section. The model was not good enough, however, to give an accurate picture of the stresses in the concentrator. Because of the shortcomings of the model used for the preliminary studies, the preliminary studies will not be discussed in detail. Instead, a more detailed description of some subsequent studies will be presented. In these subsequent studies, the approximations which lead to an overly stiff structural representation are eliminated. The

studies described in more detail concern the determination of concentrator length and the behavior of a combined concentrator and support mechanism.

CONCENTRATOR LENGTH

The study to determine concentrator length is based on the mesh shown in Figure 3. Rows of elements are added or subtracted to the length of the concentrator so that the model represents a 4.875 m (sixteen ft), 6.0 m (twenty ft), or 7.5 m (twenty-four ft) long parabolic concentrator. For all three concentrator lengths considered, the support structure is made of 0.0254 m (1.0 in) thick aluminum honeycomb with 0.508 mm (0.02 in) thick steel skins. The plates used in the model are such that the bending stiffness can be specified independently of the membrane stiffness. In addition to the plate elements, beam elements are placed along the edges and end of the concentrator. For the actual concentrator, channels are placed along the edges of the honeycomb support structure. Beam elements are included in the model to reflect the effects of the edge and end channels. Three points, those indicated in Figure 3, are constrained in the vertical direction. The rotational degrees of freedom θ_x and θ_y are also constrained at these three points. The points are free to move in the Z and X directions and to rotate about the Z-axis.

The support bonded to the thicker laminate is analyzed for three lengths. The support bonded to the thinner laminate

is analyzed for the 6.0 m concentrator. The properties of the composite sections consisting of support plus concentrator laminate are given in Appendix A. The cross-section used to approximate the channels along the edges and ends are also shown in Appendix A.

Some results obtained from putting gravity loads on the concentrator will now be discussed. For gravity acting in the -Y direction, the centerpoint deflections in the vertical direction for the support bonded to the thicker laminate are listed in Table 2. A plot of these vertical deflections (which are the maximum deflections along the vertex) versus concentrator length on log-log paper shows that deflections vary as ℓ^4, where ℓ is concentrator length (Figure 5). This is the same behavior that a simply supported beam loaded under its own weight exhibits.

Plots of stress in the upper surface of the glass are shown in Figures 6 through 13. The stresses plotted in all the figures do not account for any prestressing in the glass. Stresses arising from prestressing and thermal expansion need to be added (or subtracted) from the results plotted in the figures. A stress denoted by σ_ℓ is in the direction of the longitudinal axis of the concentrator. A stress denoted by σ_t is in the direction of a tangent to the concentrator surface that lies in a cross-section plane. The directions of σ_ℓ and σ_t for a typical quadrilateral element are shown in Figure 3.

Table 2.

Center Point Deflections for Reflector. Reflector experiences gravity load only in -y direction. Results are for a support bonded to the thicker laminate.

Reflector length-meters	Uy-meters
4.875	1.1250×10^{-4}
6.0	2.4469×10^{-4}
7.5	5.7561×10^{-4}

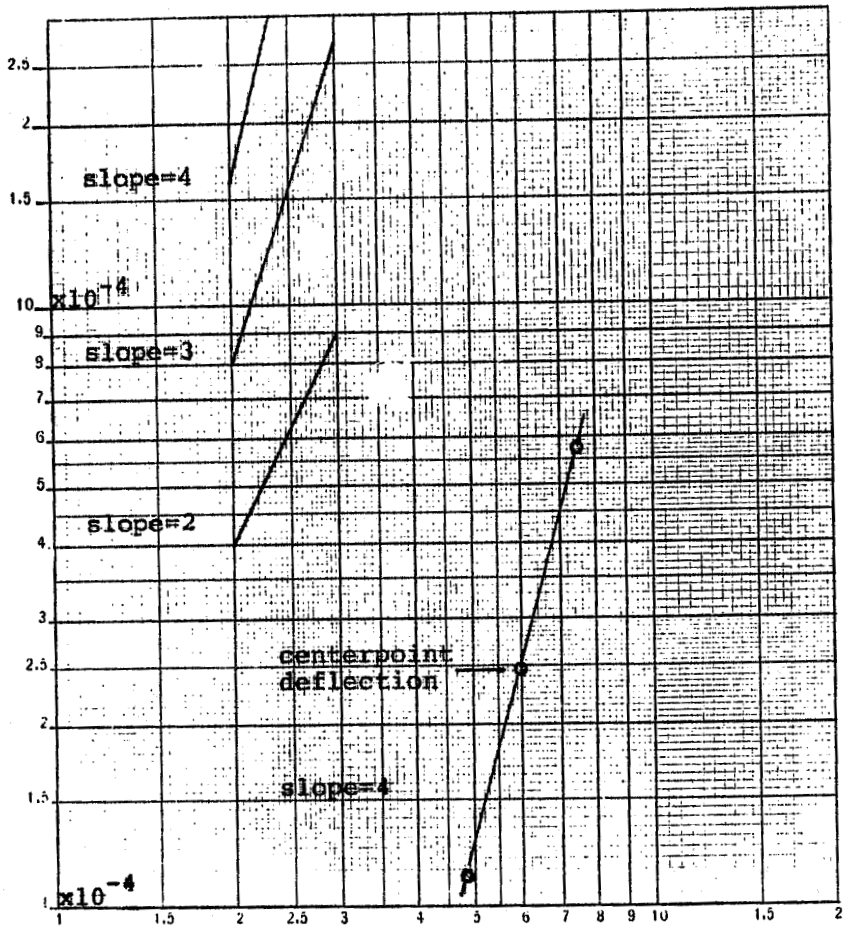

Figure 5. Plot of Centerpoint Deflections Versus Reflector Length. Reflector experiences gravity only load in -y direction. Results are for a support bonded to the thicker laminate.

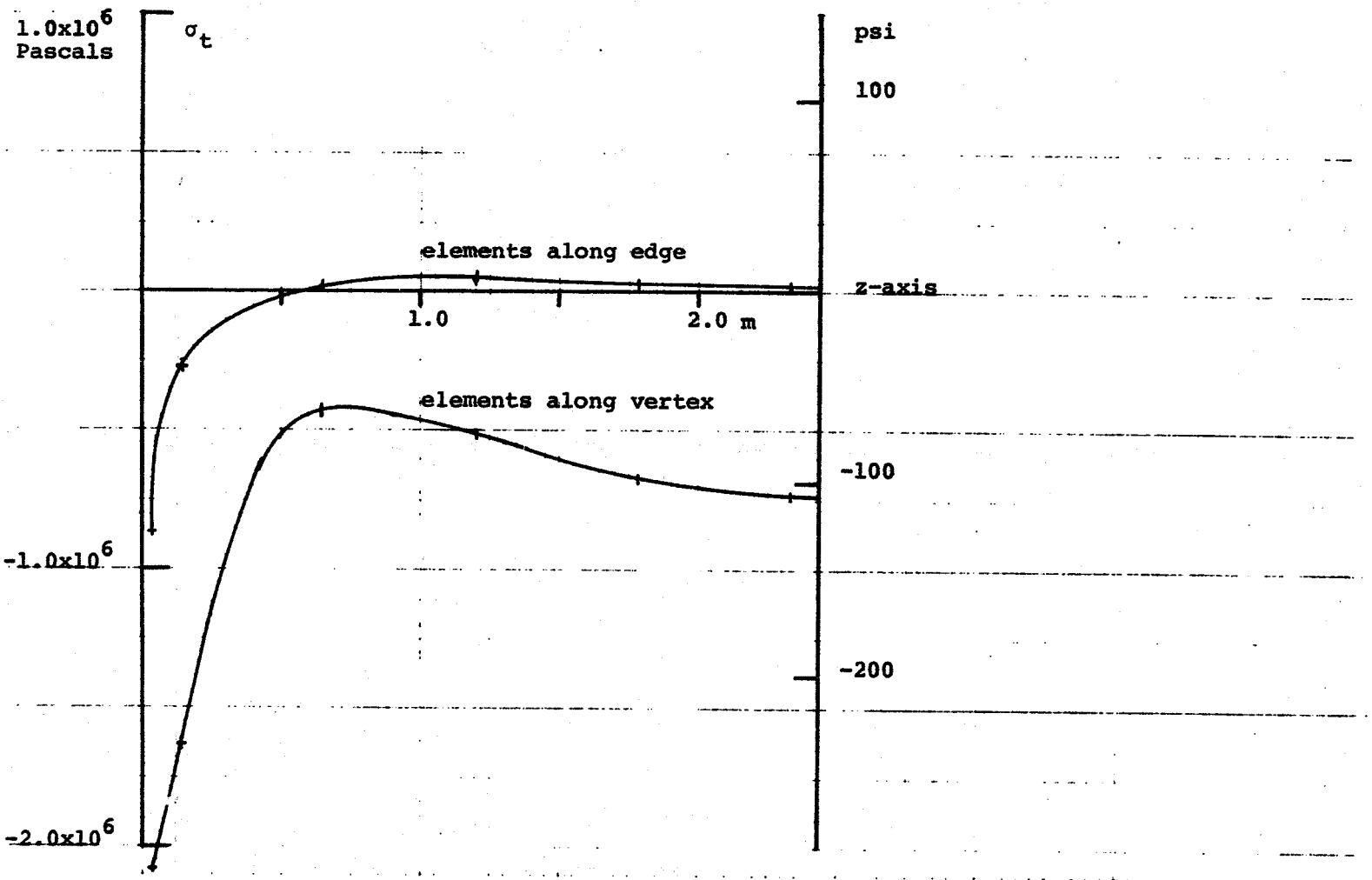

Figure 6. σ_t for edge and vertex elements of 4.875 m long concentrator. The concentrator consists of a support bonded to the thicker laminate. Gravity only acts on the concentrator in the -Y direction.

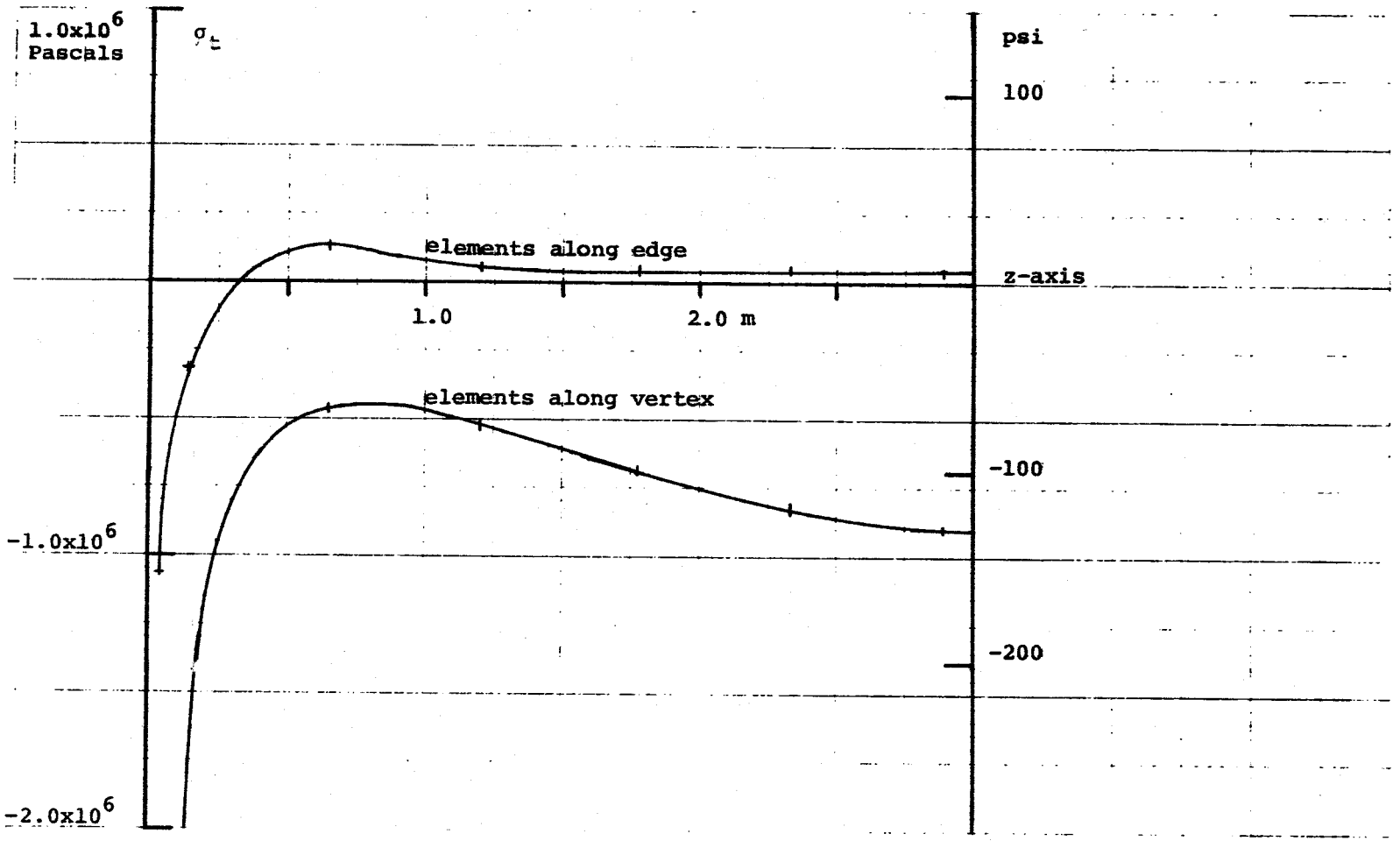

Figure 7. σ_t for edge and vertex elements of 6.0 m long concentrator. The concentrator consists of a support bonded to the thicker laminate. Gravity only acts on the concentrator in the -Y direction.

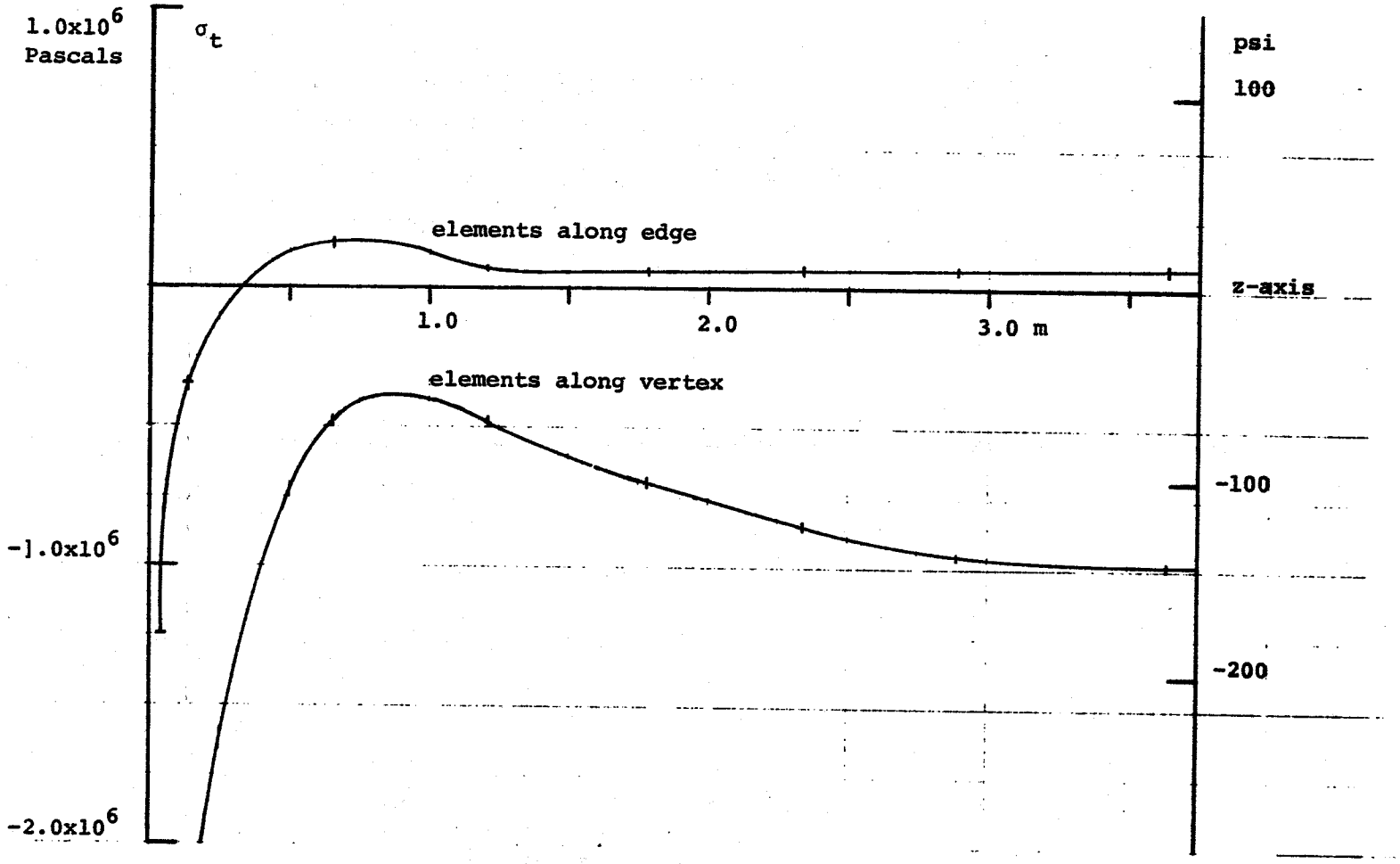

Figure 8. σ_t for edge and vertex elements of 7.5 m long concentrator. The concentrator consists of a support bonded to the thicker laminate. Gravity only acts on the concentrator in the -Y direction.

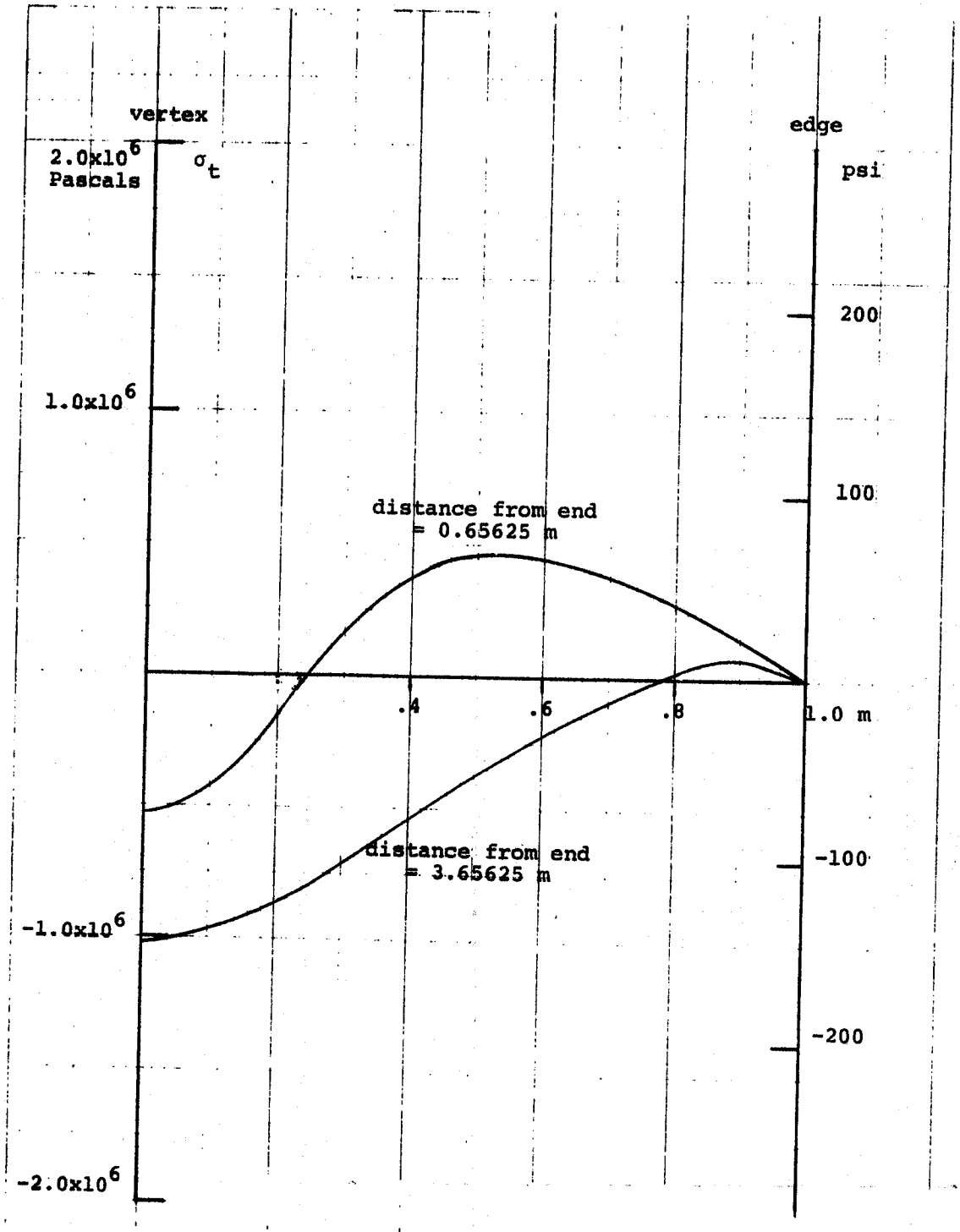

Figure 9. σ_t along cross-sections of 7.5 m long concentrator. The concentrator consists of a support bonded to the thicker laminate. Gravity only acts on the concentrator in the -Y direction.

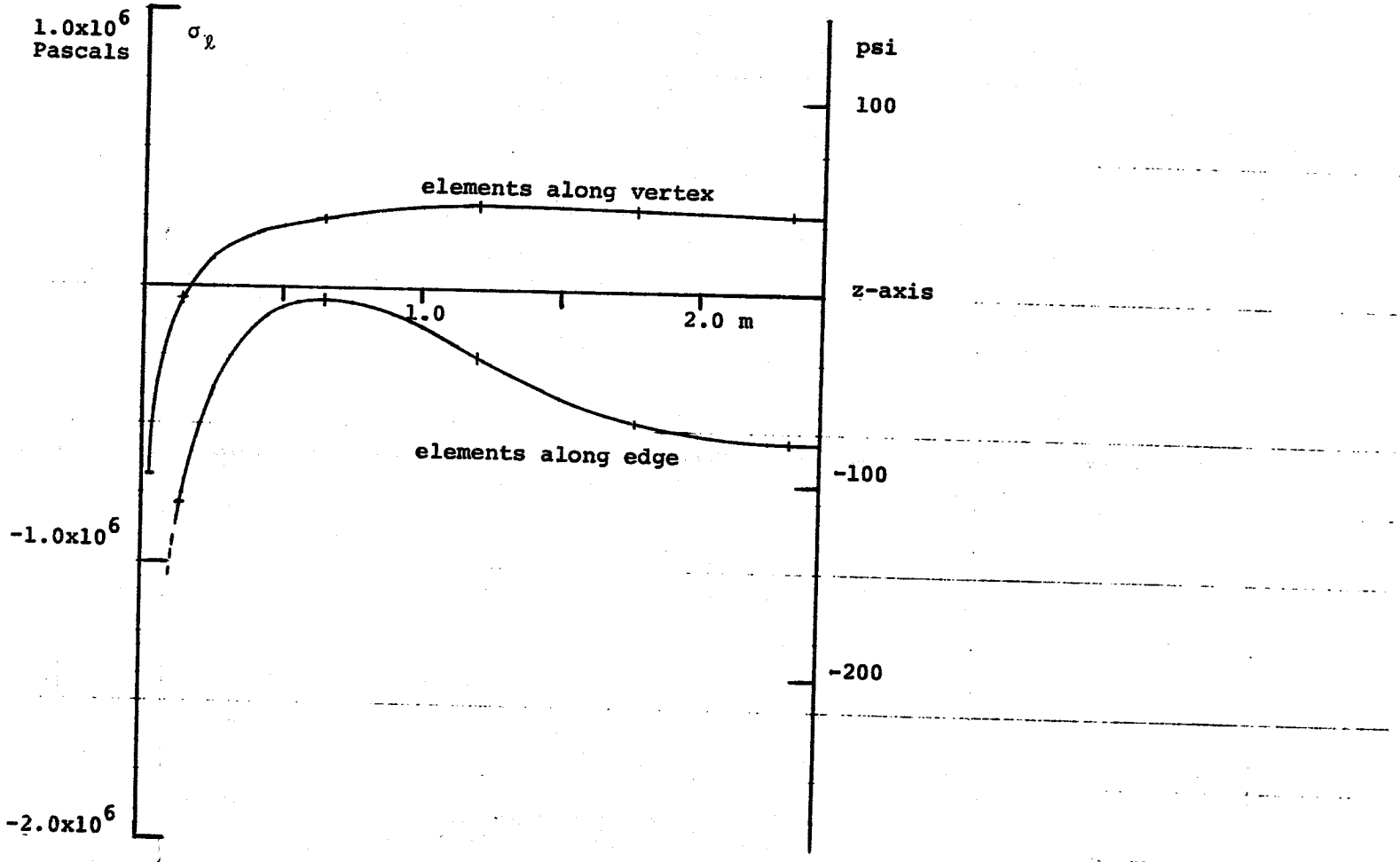

Figure 10. σ_ℓ for edge and vertex elements of 4.875 m long concentrator. The concentrator consists of a support bonded to the thicker laminate. Gravity only acts on the concentrator in the -Y direction.

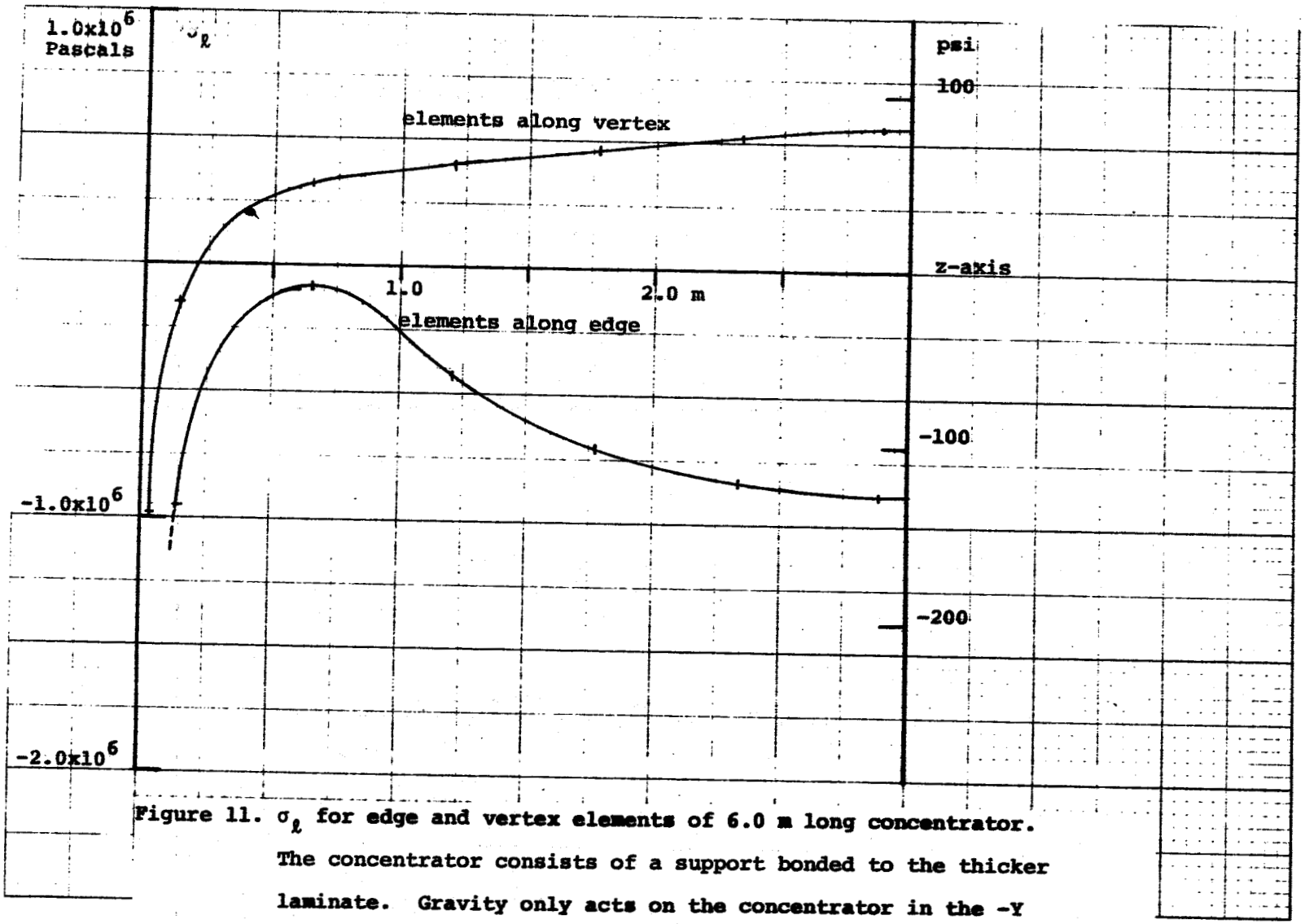

Figure 11. σ_ℓ for edge and vertex elements of 6.0 m long concentrator. The concentrator consists of a support bonded to the thicker laminate. Gravity only acts on the concentrator in the -Y direction.

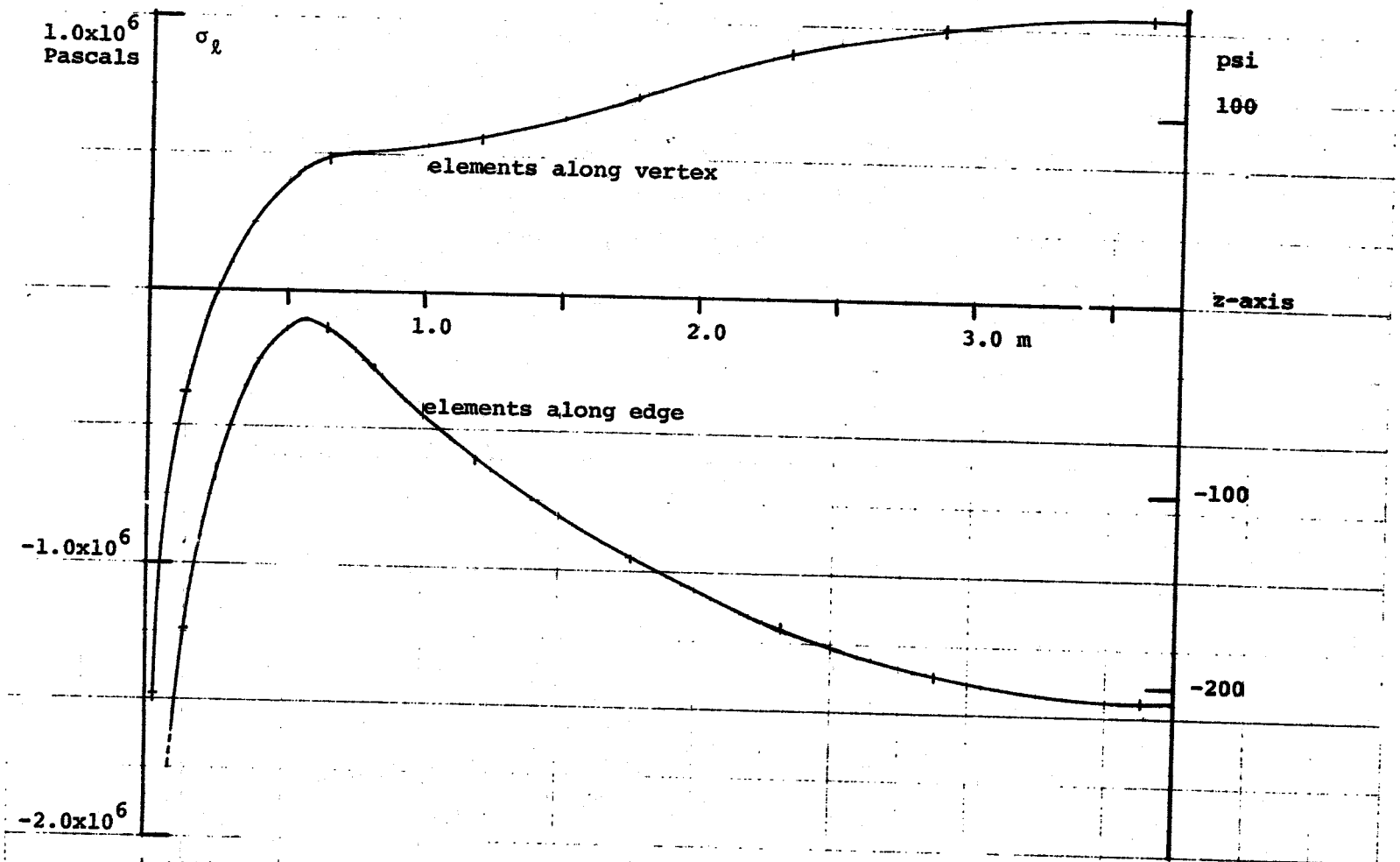

Figure 12. σ_ℓ for edge and vertex elements of 7.5 m long concentrator. The concentrator consists of a support bonded to the thicker laminate. Gravity only acts on the concentrator in the -Y direction.

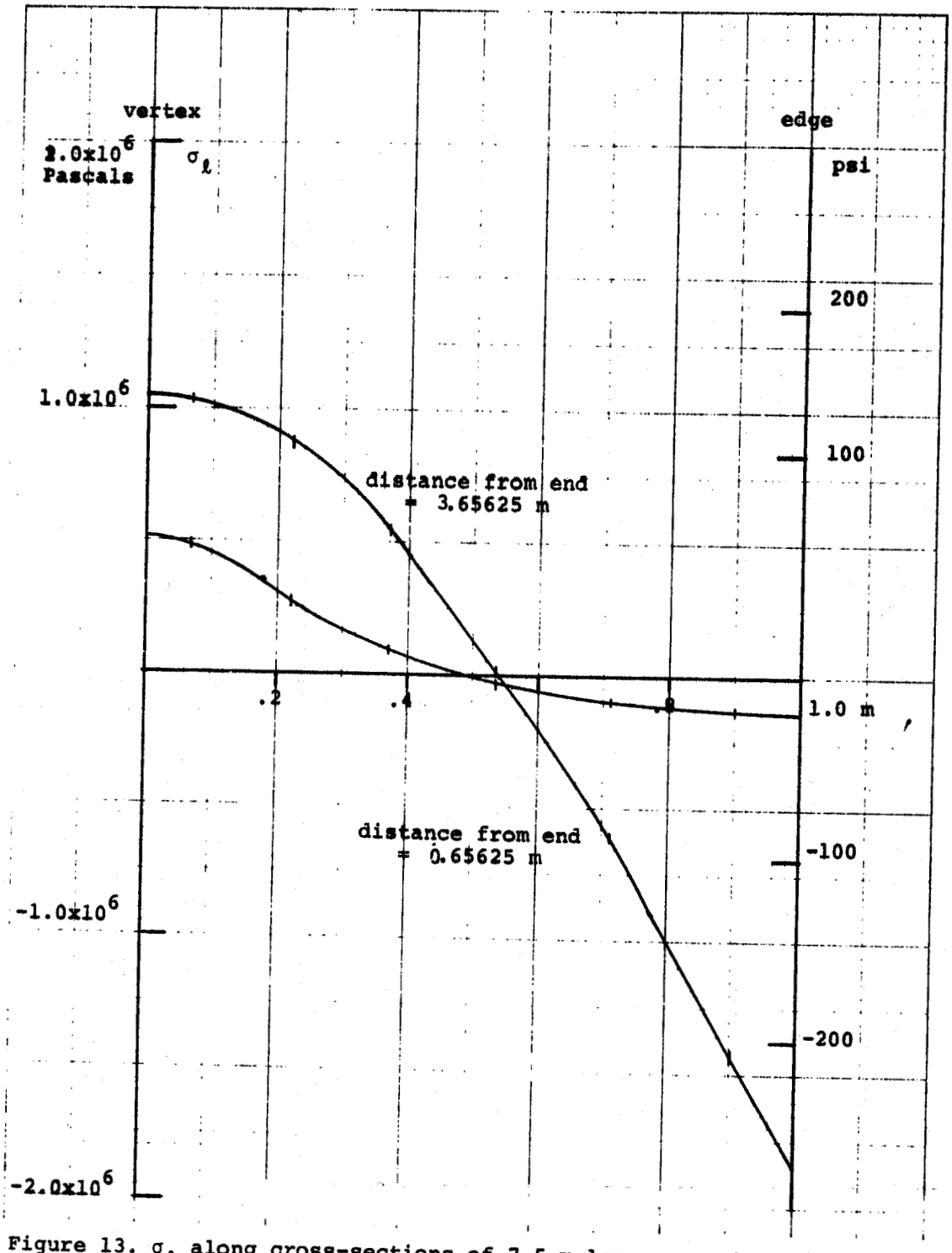

Figure 13. σ_ℓ along cross-sections of 7.5 m long concentrator. The concentrator consists of a support bonded to the thicker laminate. Gravity only acts on the concentrator in the -Y direction.

The curves depicting the stresses in the glass are based on the stresses calculated at the centroids of the plate elements in the model. Figures 6, 7, and 8 show a plot of the values of σ_t calculated at the centroids of elements along the vertex and elements along the edge. By plotting values of σ_t at various cross-sections of the parabolic concentrator, the values for σ_t can be extrapolated to the vertex and edge. At the free edge of the parabolic concentrator, the value of σ_t is zero. Figure 9 gives the plot of σ_t for two cross-sections - one close to the center cross-section and the other along a cross-section near the end region. Figures 10, 11, and 12 show a plot of the values of σ_ℓ calculated at the centroids of elements along the vertex and edge. As in the case with σ_t, values for σ_ℓ at the edge and vertex can be obtained by plotting σ_ℓ at various cross-sections. Figure 13 gives two cross-section plots of σ_ℓ. The edge and vertex values bound the values of σ_ℓ between the two cross-sections shown. The values for σ_t and σ_ℓ in all instances are inaccurate near the supported end of the concentrator. The support points generate stress concentrations in the concentrator, and the mesh is not accurate enough to model these concentrations in detail. As a result, some of the elements near the end of the concentrator have large gradients across them and predict excessively large stresses.

Stresses in the upper surfaces of the glass for the 6.0 m long concentrator made up of the support bonded to the

thinner laminate are shown in Figures 14 through 17. These results are also for the case of gravity acting in the -Y direction. The thinner laminate has little effect on the σ_t stresses, as can be seen by comparing Figures 7 and 14. The σ_ℓ stresses near the center cross-section go up by approximately thirty percent, however, for the case with the thinner laminate. This is evident when one compares Figures 11 and 16. Figures 15 and 17 are cross-section plots.

Stresses in the glass serve as one means of evaluating the structure. Another means of evaluating the structure is by calculating equivalent slope errors for various points on the surface of the trough when it undergoes deflections due to wind and gravity loads. The equivalent slope error for a point undergoing deflections Δx and Δy and rotation δ in a cross-sectional plane (Figure 18) is given by

$$\Delta/R_1 = [2\delta + [\Delta x\, x_1 - \Delta y\, (f - y_1)]/R_1^2]. \qquad (1)$$

In equation 1, x_1 and y_1 are the original coordinates of the point of interest, f is the focal length of the parabola, and R_1 is given by

$$R_1 = [x_1^2 + (f - y_1)^2]^{1/2}.$$

The quantity R_1 is the distance from the focal point to the point of interest.

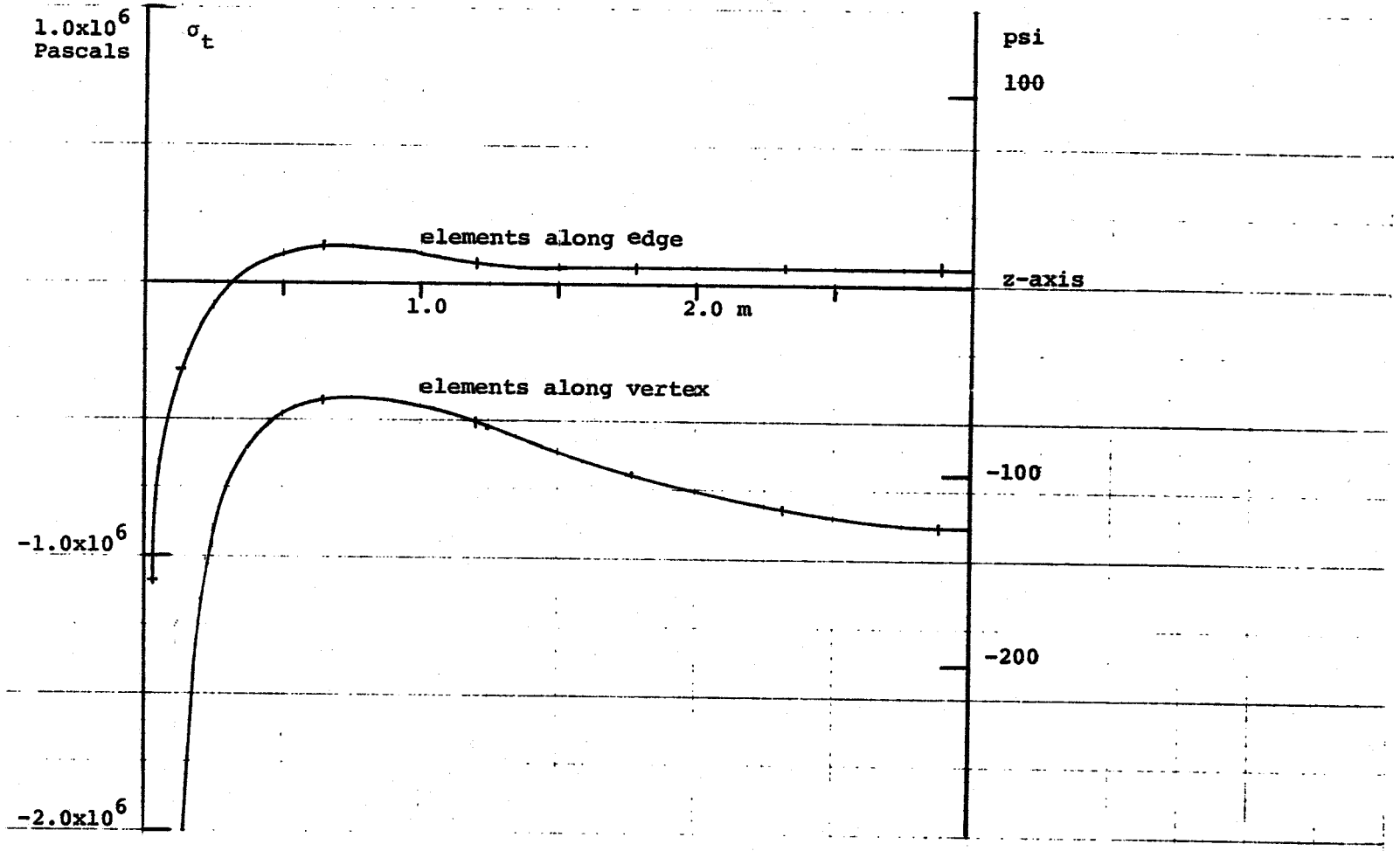

Figure 14. σ_ℓ for edge and vertex elements of 6.0 m long concentrator. The concentrator consists of a support bonded to the thinner laminate. Gravity only acts on the concentrator in the -Y direction.

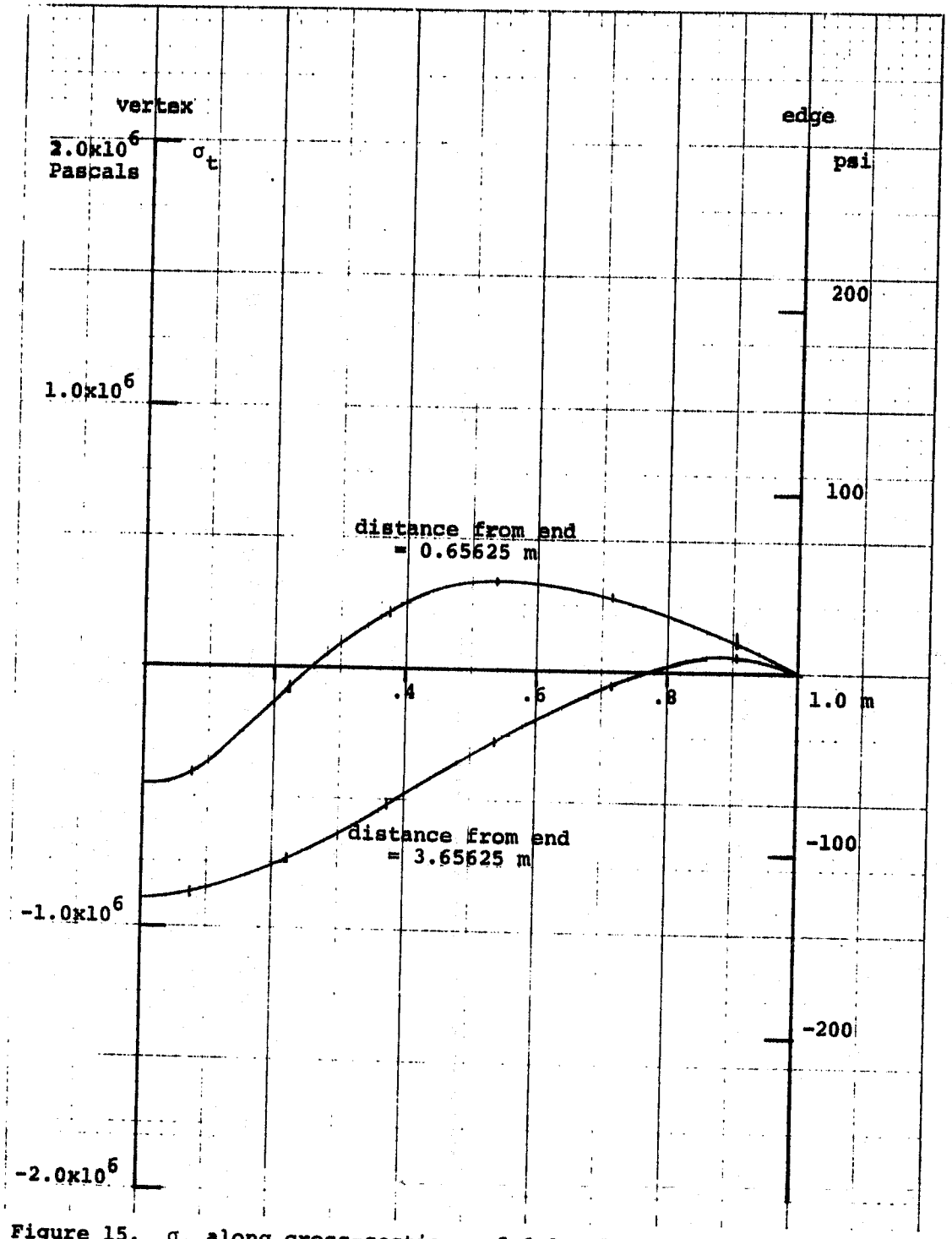

Figure 15. σ_ℓ along cross-sections of 6.0 m long concentrator. The concentrator consists of a support bonded to the thinner laminate. Gravity only acts on the concentrator in the -Y direction.

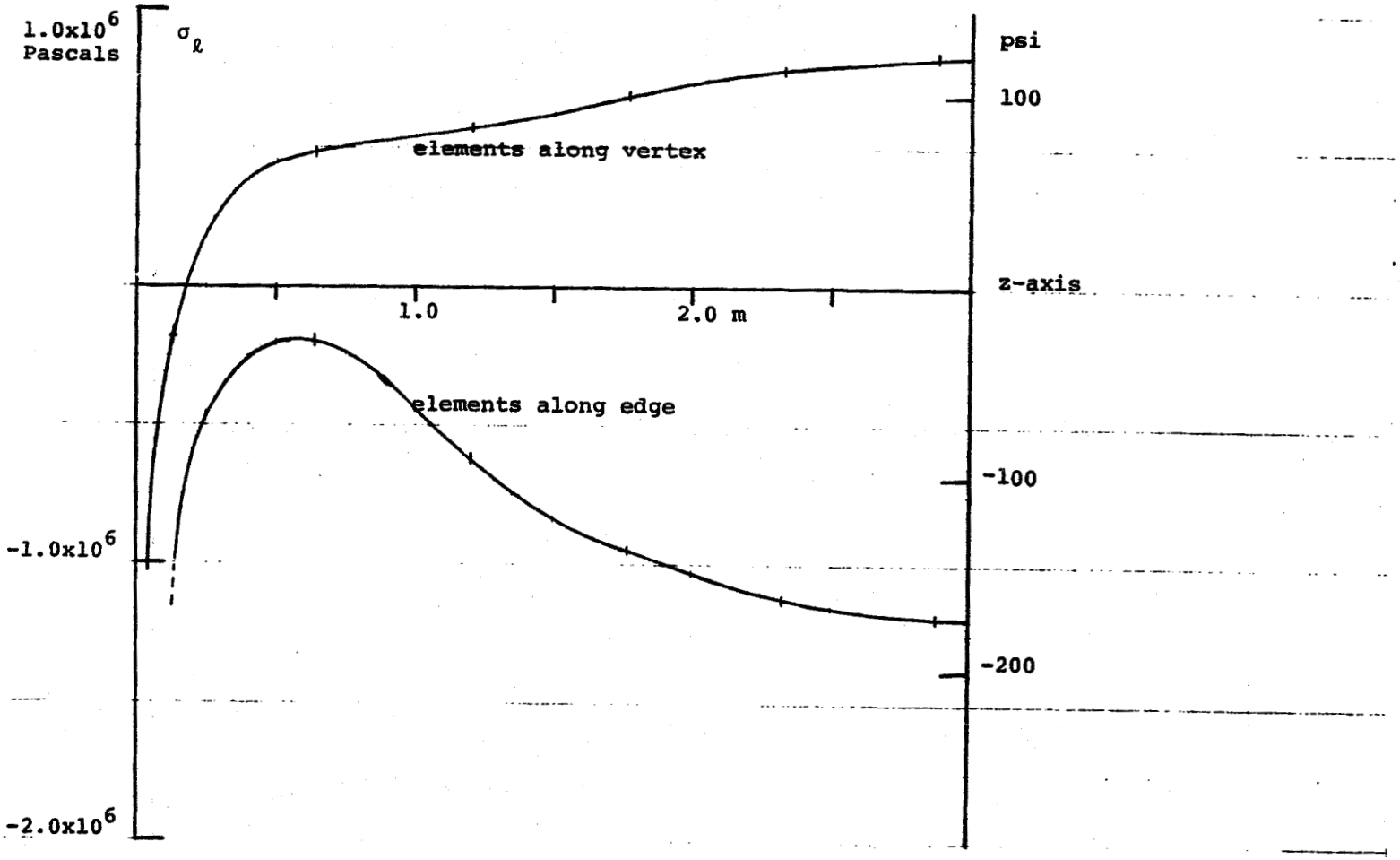

Figure 16. σ_ℓ for edge and vertex elements of 6.0 m long concentrator. The concentrator consists of a support bonded to the thinner laminate. Gravity only acts on the concentrator in the -Y direction.

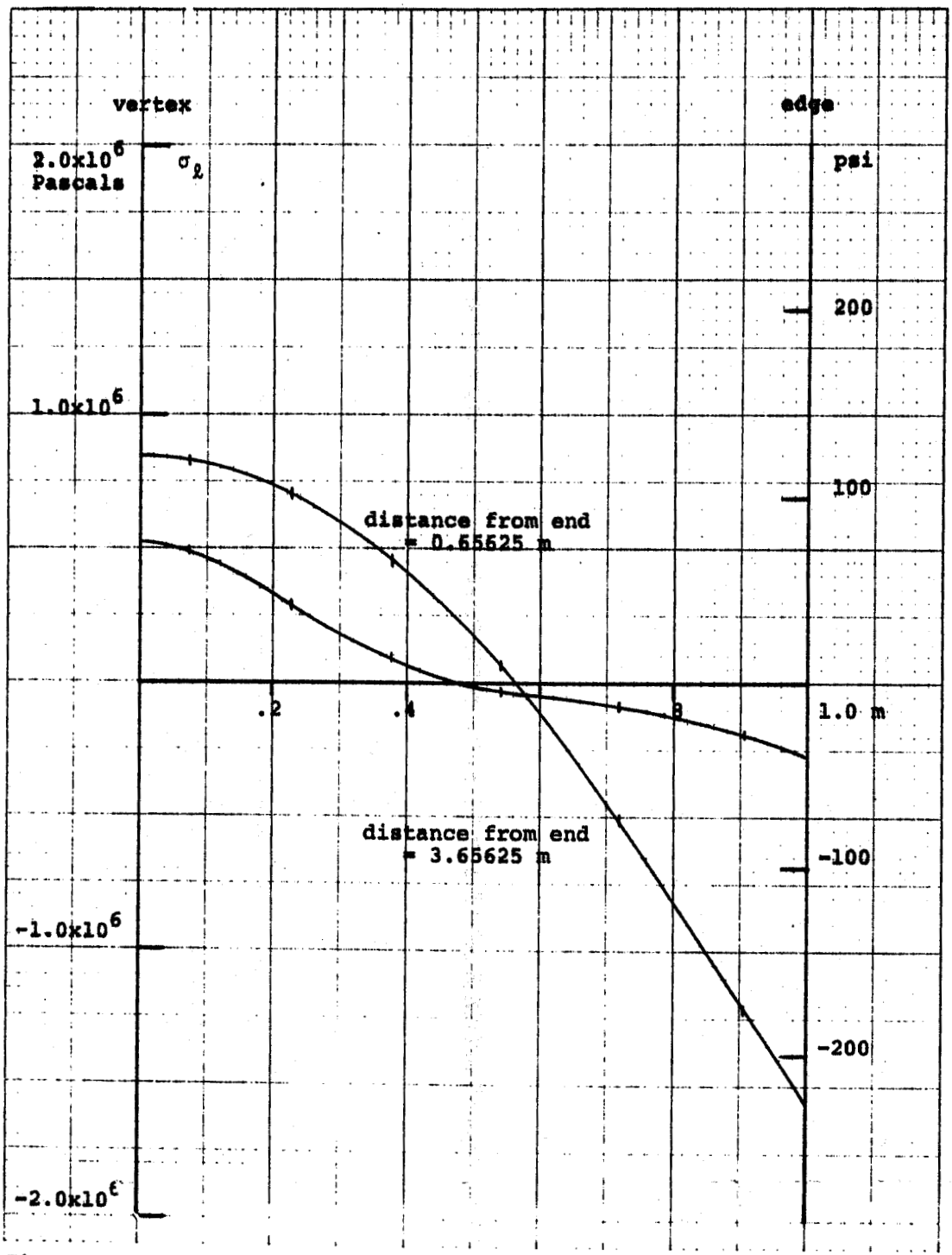

Figure 17. σ_ℓ along cross-sections of 6.0 m long concentrator. The concentrator consists of a support bonded to the thinner laminate. Gravity only acts on the concentrator in the -Y direction.

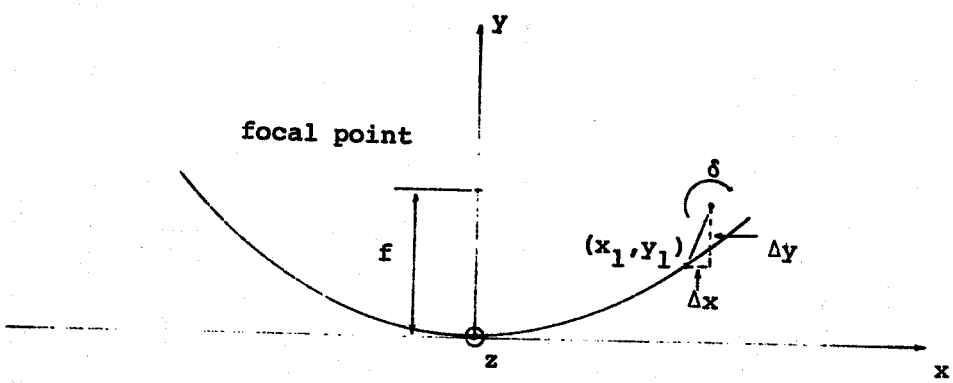

Figure 18. Notation for Equivalent Slope Errors

Tables 3 and 4 show some equivalent slope errors for the 7.5 m long concentrator (made of the support bonded to the thicker laminate) for two loading conditions. The results in Table 3 are for the case where the concentrator is tilted forty-five degrees from the X-Z plane. The trough is subjected to combined wind and gravity loads as shown in Figure 19. The pressure distribution across the aperture of the concentrator for a 13.41 mps (thirty mph) wind is also shown in Figure 19. This distribution varies linearly across the aperture and produces a moment similar to that which arises from wind tunnel results for a concentrator tilted at a similar angle to the wind.

The concentrator must be designed so that in the 13.41 mps wind, the equivalent slope error Δ/R_1 is less than 6.0 milliradians. The computer studies indicate that the 7.5 m long concentrator can meet this requirement. For the 7.5 m length, however, it appears that the glass stresses will be excessive in a 40.23 mps (ninety mph) wind. The 6.0 m long concentrator will easily meet the slope error requirements for a 13.41 mps (thirty mph) wind, and the glass stresses in the survival wind conditions (40.23 mps) will be appreciably lower than those in the 7.5 m concentrator. Based on these considerations, it is desirable to examine the 6.0 m long concentrator in greater detail, i.e., with a refined mesh in the attachment region and a support mechanism included in the model. The next section discusses a more

Table 3.

Slope Errors for 7.5 m Long Reflector Subject to Gravity Load in -y Direction. The reflector is made up of the support bonded to the thicker laminate.

Location			Deflections			Slope Error/R_1
$x^{(1)}$-meters	$y^{(2)}$-meters	z-meters	Δx-meters	Δy-meters	δ-radians	Δ/R_1
0.0	-0.4828	3.75	0.0	-5.76×10^{-4}	0.0	0.0
0.1916	-0.4638	3.75	4.06×10^{-6}	-5.88×10^{-4}	1.28×10^{-4}	-1.92×10^{-4}
0.3765	-0.4095	3.75	9.78×10^{-6}	-6.22×10^{-4}	2.37×10^{-4}	-2.96×10^{-4}
0.5502	-0.3261	3.75	3.27×10^{-5}	-6.71×10^{-4}	3.16×10^{-4}	-2.96×10^{-4}
0.7116	-0.2207	3.75	6.87×10^{-5}	-7.26×10^{-4}	3.63×10^{-4}	-2.32×10^{-4}
0.8611	-0.0989	3.75	1.15×10^{-4}	-7.82×10^{-4}	3.85×10^{-4}	-1.41×10^{-4}
1.0000	0.0349	3.75	1.68×10^{-4}	-8.35×10^{-4}	3.93×10^{-4}	-4.10×10^{-5}

(1) $x_1 = x$

(2) $y_1 = y + f = y + 0.4828$

Table 4.

Slope Errors for 7.5 m Long Reflector Subject to Combined Wind and Gravity Loads. The reflector is made up of the support bonded to the thicker laminate.

Location			Deflections			Slope error/R_1
$x^{(1)}$-meters	y-meters	z-meters	Δx-meters	Δy-meters	δ-radians	Δ/R_1
0.0	-0.4828	3.75	2.44×10^{-4}	-6.20×10^{-4}	1.71×10^{-3}	2.91×10^{-3}
0.1916	-0.4638	3.75	2.77×10^{-4}	-9.64×10^{-4}	1.87×10^{-3}	2.50×10^{-3}
0.3765	-0.4095	3.75	3.81×10^{-4}	-1.32×10^{-3}	2.02×10^{-3}	1.92×10^{-3}
0.5502	-0.3261	3.75	5.53×10^{-4}	-1.68×10^{-3}	2.12×10^{-3}	1.54×10^{-3}
0.7116	-0.2207	3.75	7.80×10^{-4}	-2.03×10^{-3}	2.19×10^{-3}	1.46×10^{-3}
0.8611	-0.0989	3.75	1.05×10^{-3}	-2.36×10^{-3}	2.22×10^{-3}	1.59×10^{-3}
1.000	0.0349	3.75	1.35×10^{-3}	-2.67×10^{-3}	2.24×10^{-3}	1.87×10^{-3}

(1) $x_1 = x$

(2) $y_1 = y + f = y + 0.4828$

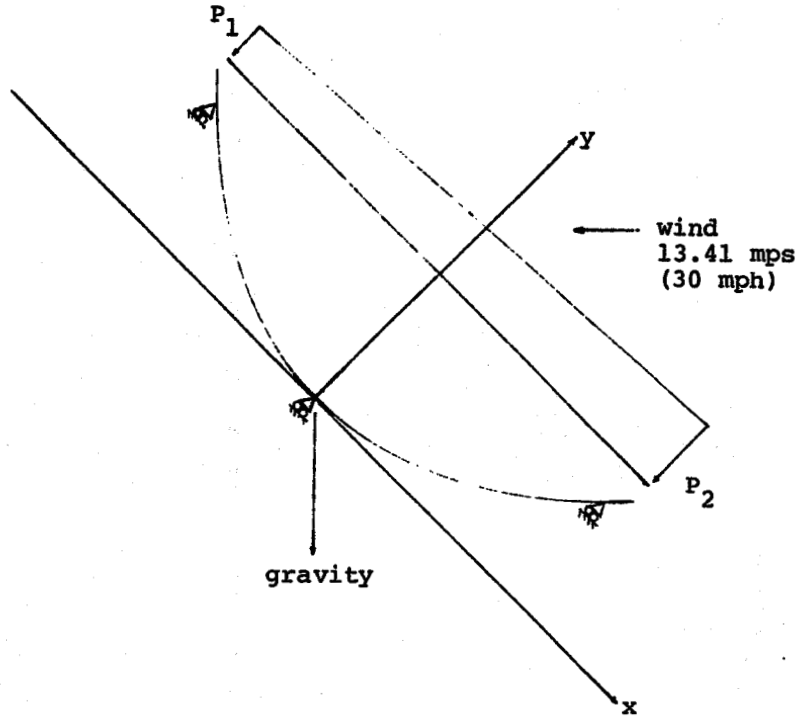

P_1 = 55.16 Pascals
P_2 = 110.32 Pascals

Figure 19. Combined Wind and Gravity Load Configuration Used on 7.5 m Long Reflector for Slope Error Study

detailed study of a 6.0 m long concentrator.

6.0 m LONG CONCENTRATOR COMBINED WITH SUPPORT MECHANISM

The mesh for the 6.0 m long concentrator is shown in Figure 20. The view in Figure 20 shows the mesh for the concentrator in a flattened shape. None of the support structure is shown. More data is given for the mesh in Appendix B. Appendix B shows the mesh for the support mechanism combined with the concentrator.

Two loading configurations are presented in detail for the combination concentrator-support mechanism. For the first loading configuration, the concentrator is pointing in the +Y direction and gravity is acting in the -Y direction. Symmetry conditions are imposed on the support pylon, so that the pylon appears to have a concentrator mounted on either side of it. Deformed shapes for this particular loading are shown in Figures 21 through 23.

Figures 24 and 25 show plots of stresses in elements along the vertex and along the edge. The value of σ_ℓ near the center cross-section is larger for the concentrator-support mechanism combination than for the concentrator by itself. This is evident when one compares Figure 25 with Figure 11. The differences in the σ_ℓ stresses have to do with the different support mechanisms in the two models. The support points for the model shown in Figure 3 have several degrees of freedom rigidly constrained. For the concentrator-support

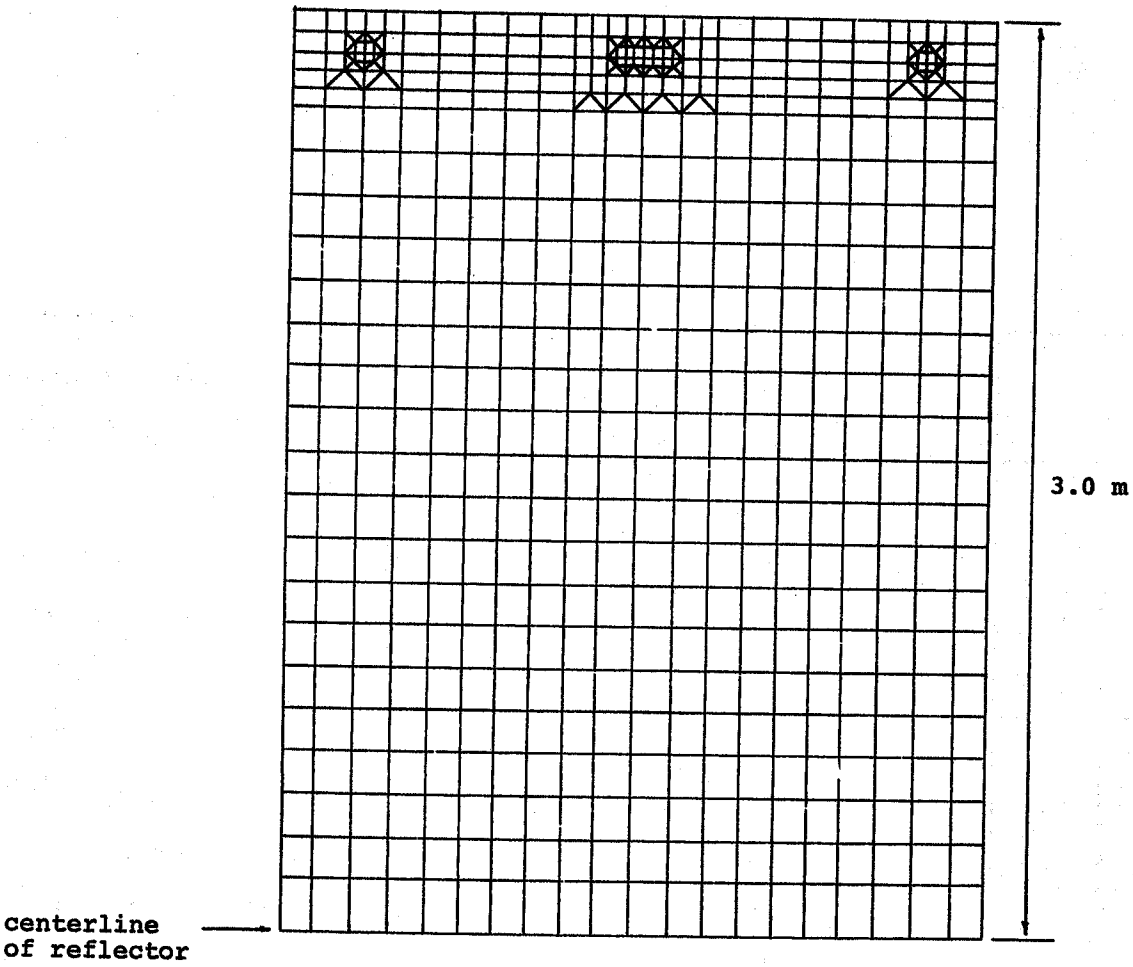

Figure 20. Mesh Used for Reflector in Combined Reflector - Support Mechanism Studies

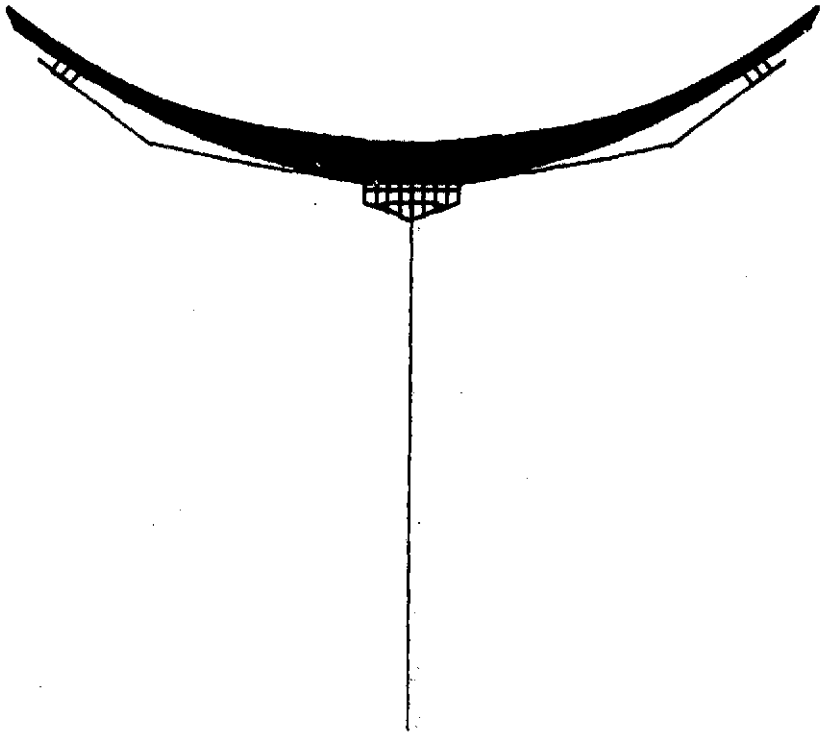

Figure 21. 6.0 m Long Reflector with Support Mechanism under Gravity Load - End View; Symmetry Conditions on Support Pylon

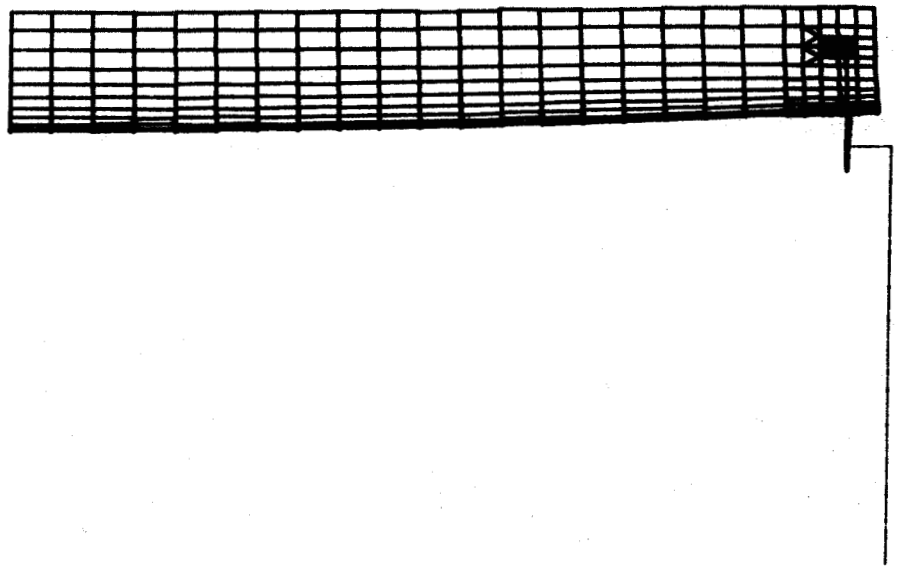

Figure 22. 6.0 m Long Reflector with Support Mechanism under Gravity Load - Side View; Symmetry Conditions on Support Pylon

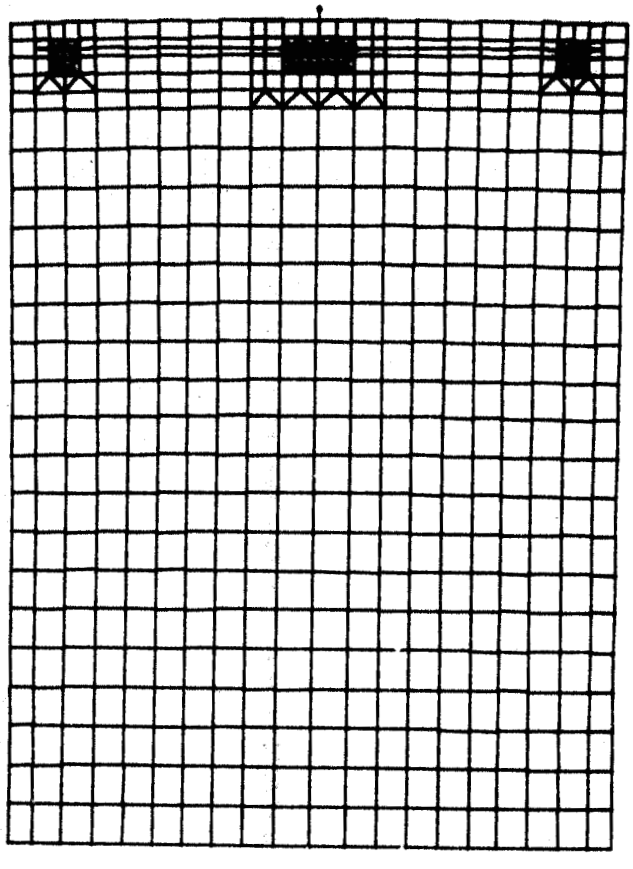

Figure 23. 6.0 Long Reflector with Support Mechanism under Gravity Load - Top View; Symmetry Conditions on Support Pylon

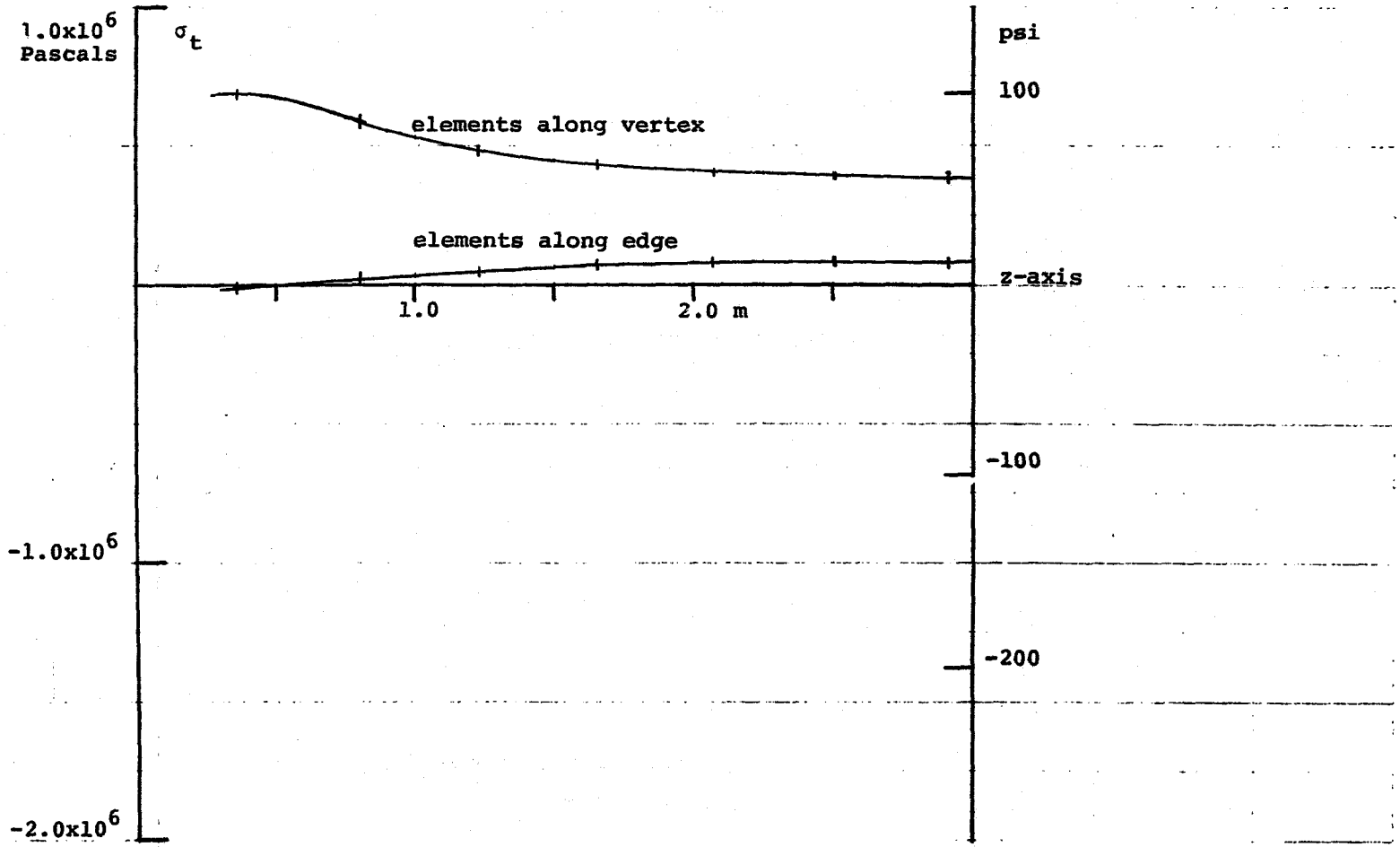

Figure 24. σ_t for edge and vertex elements of 6.0 m long concentrator with support mechanism. The concentrator consists of a support bonded to the thicker laminate. Gravity only acts on the concentrator in the -Y direction.

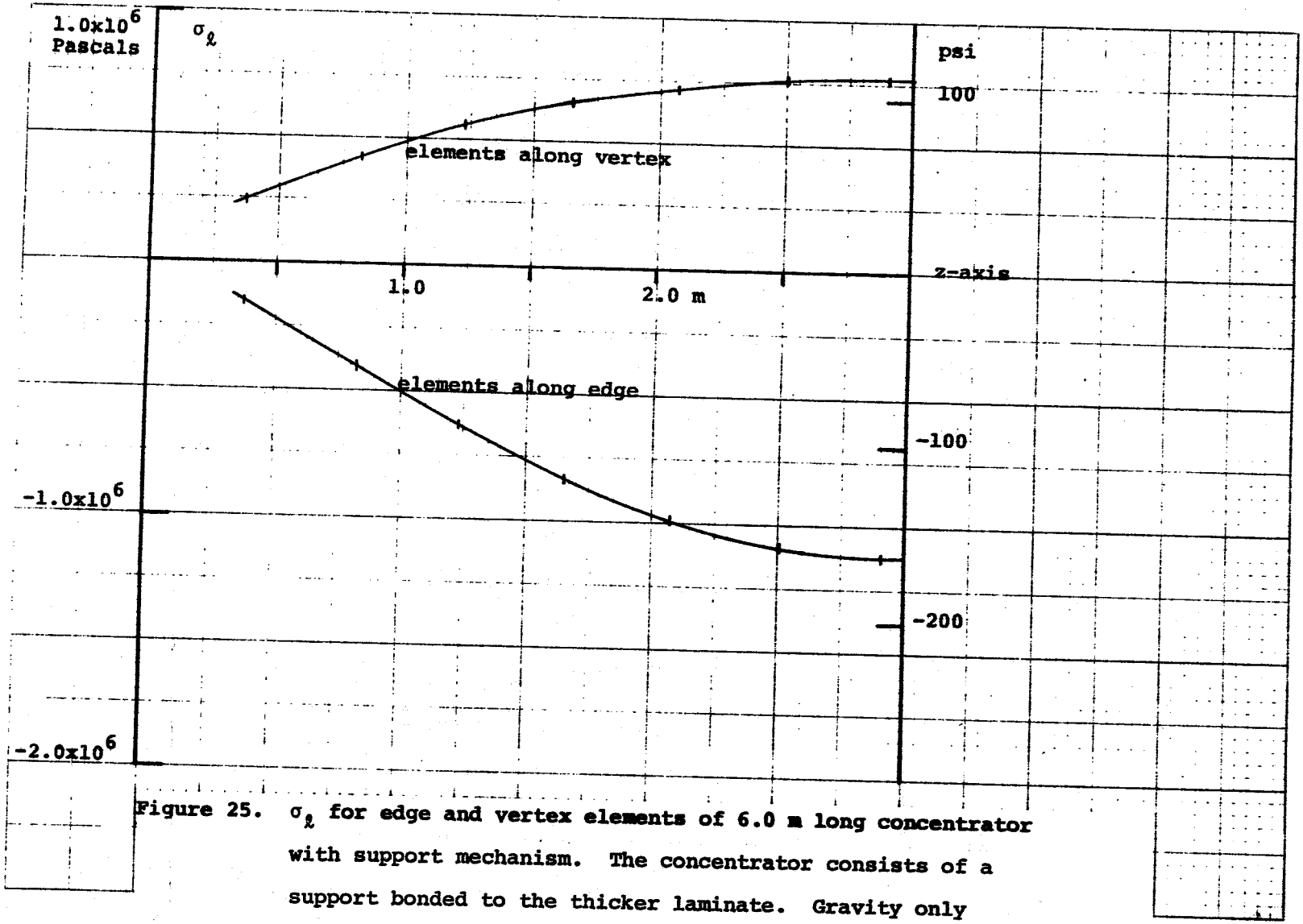

Figure 25. σ_ℓ for edge and vertex elements of 6.0 m long concentrator with support mechanism. The concentrator consists of a support bonded to the thicker laminate. Gravity only acts on the concentrator in the -Y direction.

mechanism, none of the support points on the concentrator are rigidly constrained. All degrees of freedom associated with the attachment points between the concentrator and support mechanism have some flexibility. Increasing the flexibility at the support points on the concentrator produces greater values for the stress σ_ℓ.

Plots of stresses in the regions surrounding the attachment points are shown in Figures 26 through 30. Stress concentrations occur near the attachment points. Figures 26 through 29 show plots of σ_t with increasing distance from the attachment points. The concentrations decay rather rapidly as one moves away from the attachment points. The attachment points are located along a cross-section that is 0.9525 m (3.75 in) from the end of the concentrator. A plot of σ_ℓ at a cross-section 0.127 m (5.0 in) from the end of the concentrator is shown in Figure 30. The magnitudes of the concentrations for σ_t are larger than those for σ_ℓ.

The first loading condition is also studied for the case where there are no symmetry conditions on the support pylon. Symmetry conditions left on the center section of the concentrator simulate the case of a single concentrator loaded symmetrically about its center cross-section. The deformed configurations for this case are shown in Figures 31 through 33. A plot of the σ_ℓ stresses for elements along the edge and vertex are shown in Figure 34. The maximum value for σ_ℓ is slightly larger than the maximum value for σ_ℓ shown in

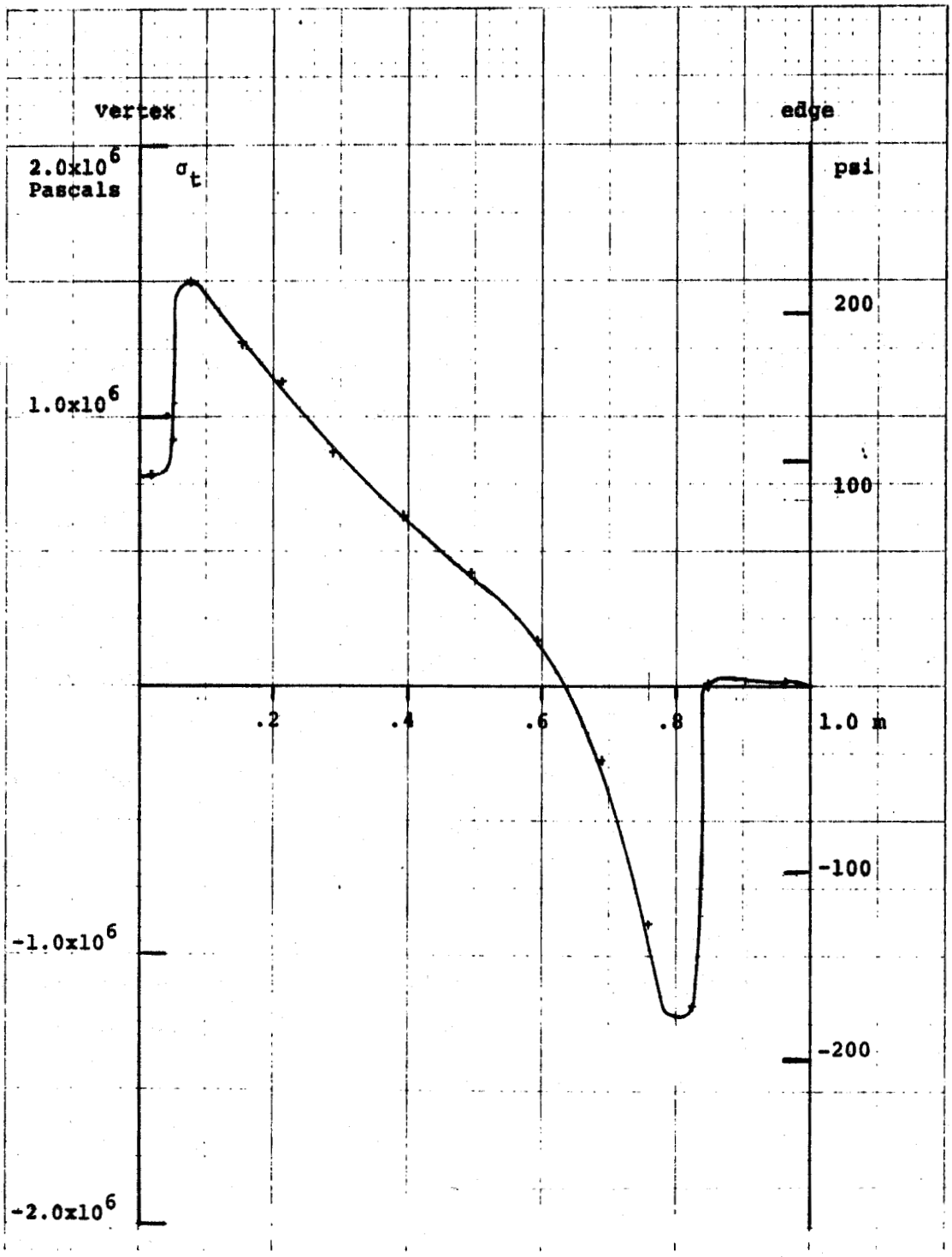

Figure 26. σ_t along cross-section of 6.0 m long concentrator with support mechanism. The concentrator consists of a support bonded to the thicker laminate. Gravity only acts on the concentrator in the -Y direction. The cross-section shown is 0.127 m (5.0 in) from the end of the concentrator.

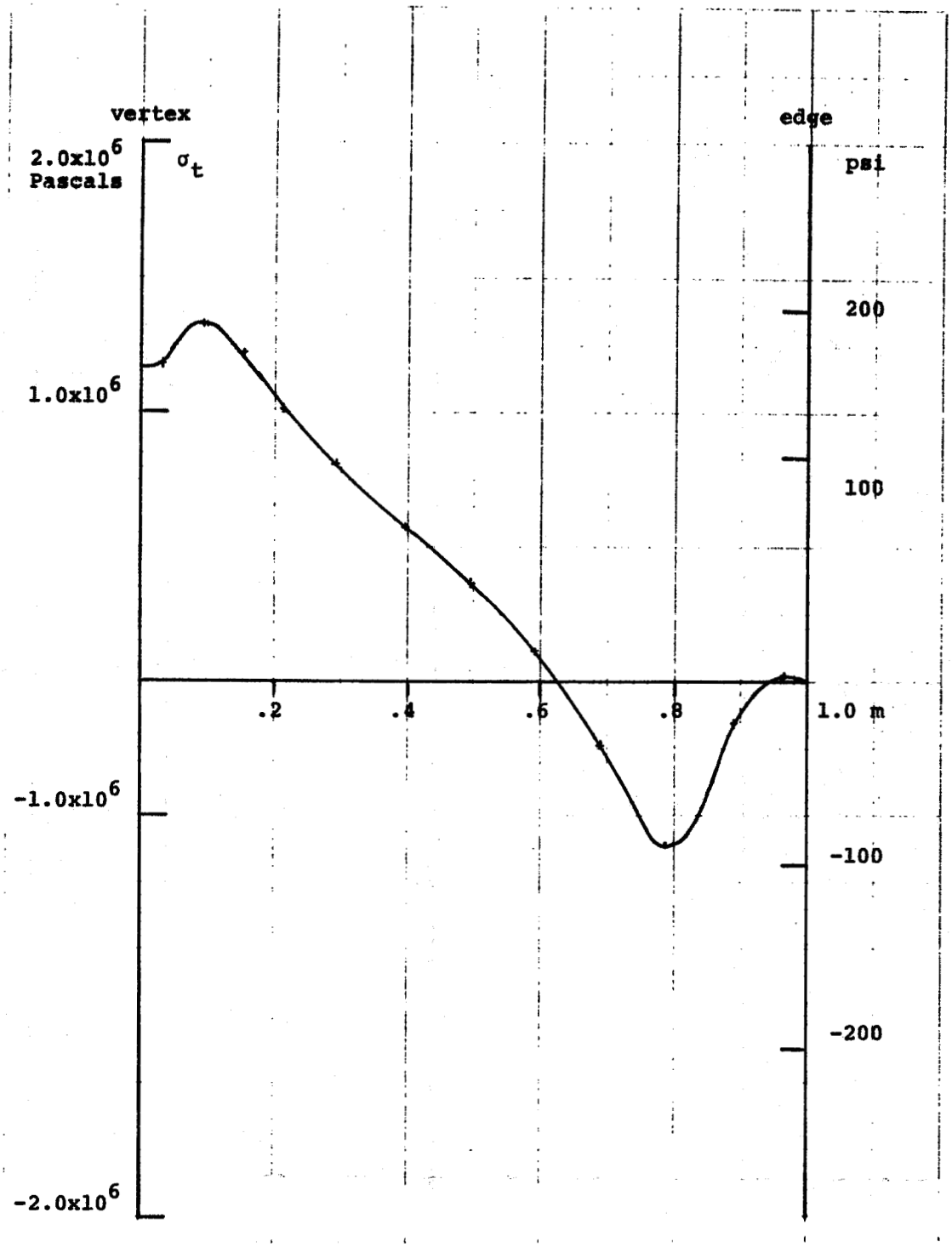

Figure 27. σ_t along cross-section of 6.0 m long concentrator with support mechanism. The concentrator consists of a support bonded to the thicker laminate. Gravity only acts on the concentrator in the -Y direction. The cross-section shown is 0.22225 m (8.75 in) from the end of the concentrator.

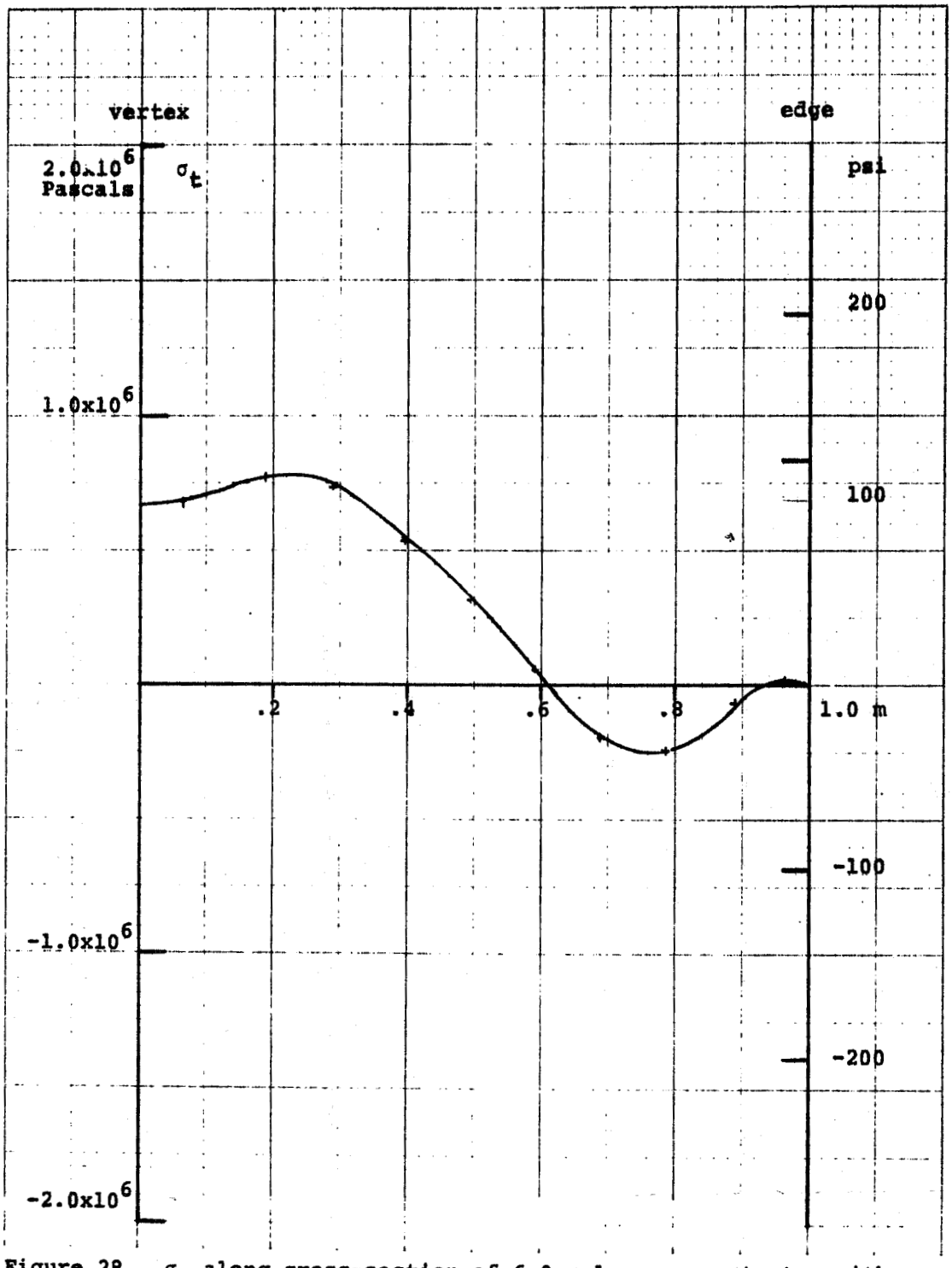

Figure 28. σ_t along cross-section of 6.0 m long concentrator with support mechanism. The concentrator consists of a support bonded to the thicker laminate. Gravity only acts on the concentrator in the -Y direction. The cross-section shown is 0.28575 m (11.25 in) from the end of the concentrator.

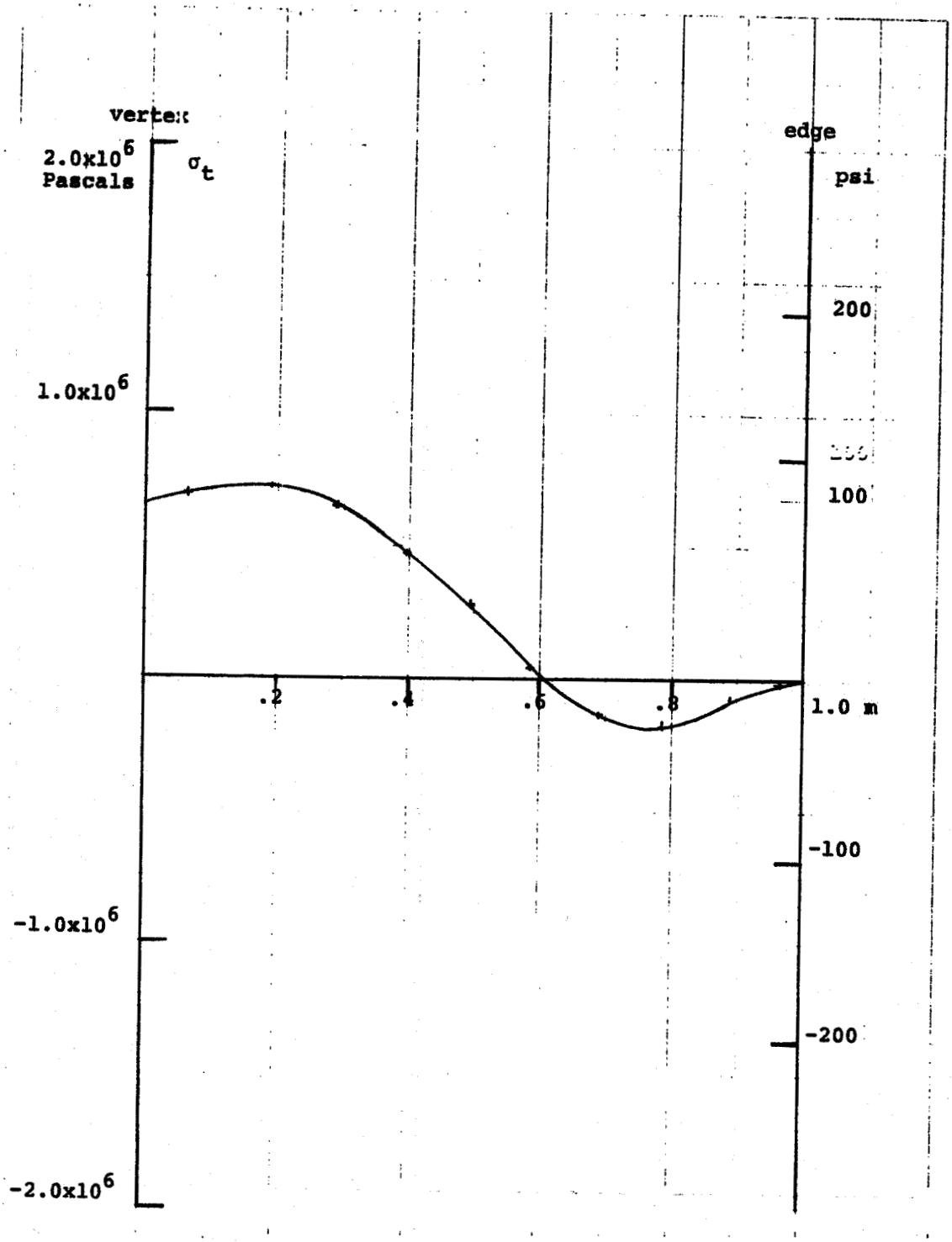

Figure 29. σ_t along cross-section of 6.0 m long concentrator with support mechanism. The concentrator consists of a support bonded to the thicker laminate. Gravity only acts on the concentrator in the -Y direction. The cross-section shown is 0.38809 m (15.28 in) from the end of the concentrator.

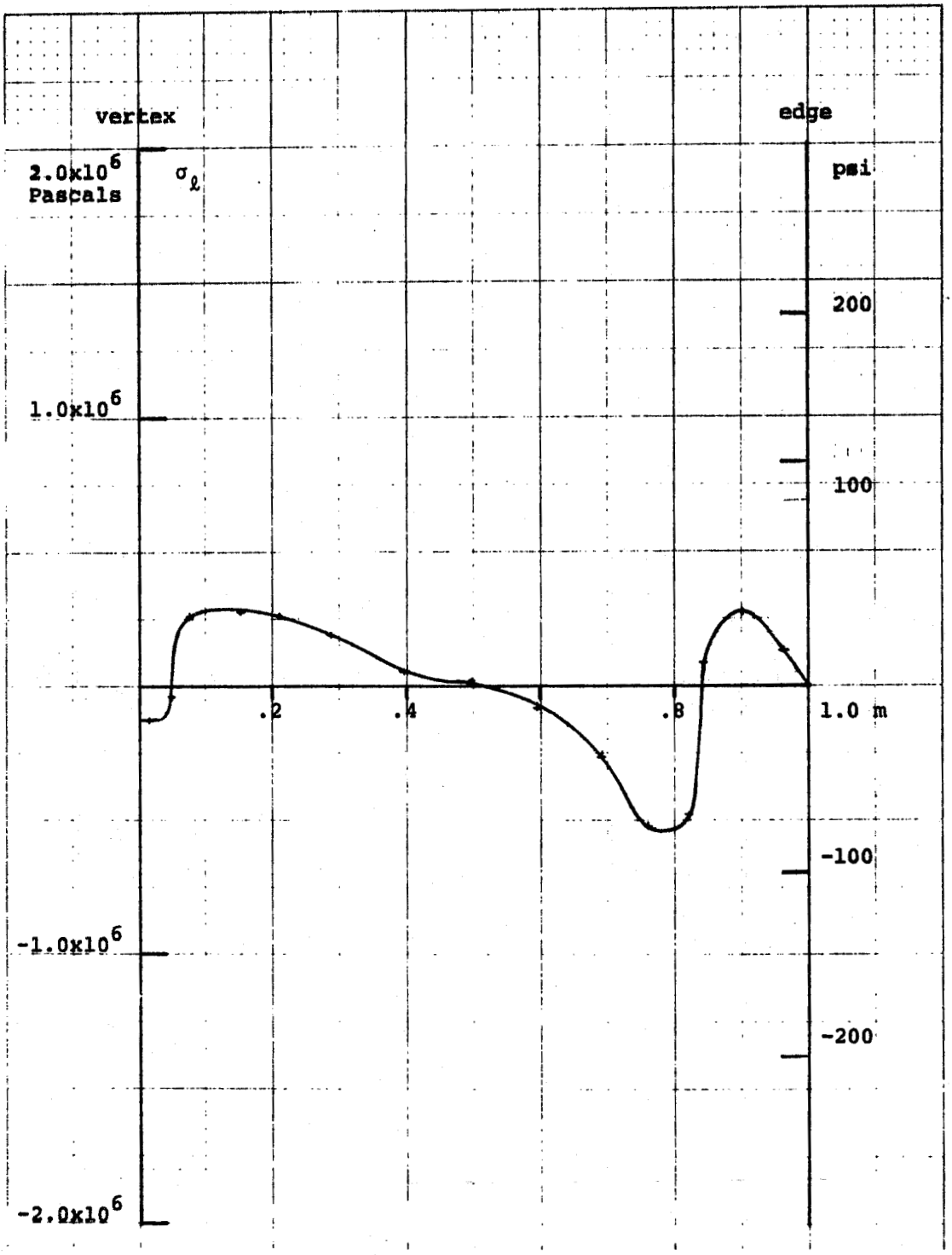

Figure 30. σ_t along cross-section of 6.0 m long concentrator with support mechanism. The concentrator consists of a support bonded to the thicker laminate. Gravity only acts on the concentrator in the -Y direction. The cross-section shown is 0.127 m (5.0 in) from the end of the concentrator

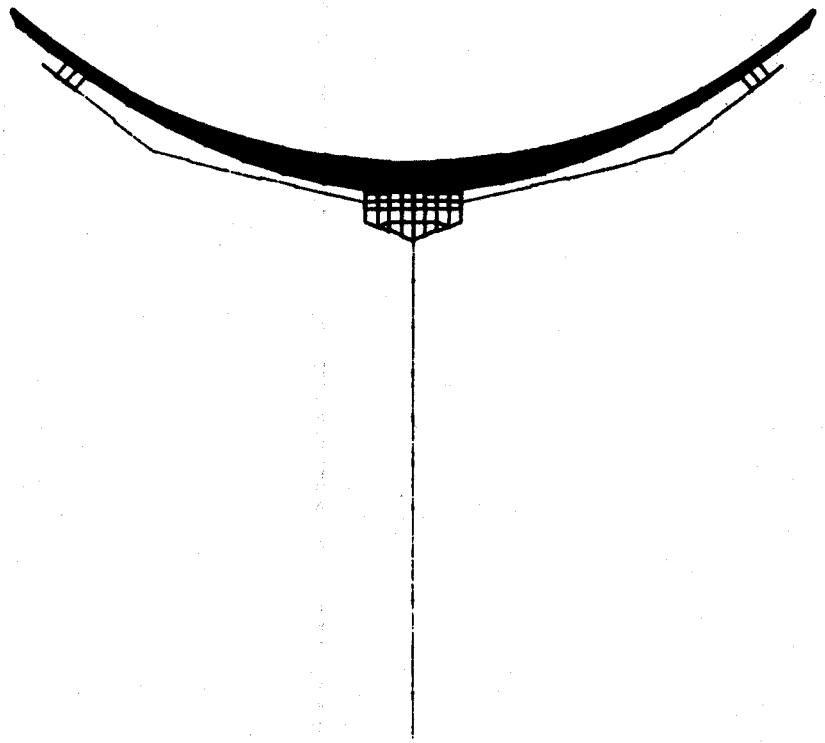

Figure 31. 6.0 m Long Reflector with Support Mechanism under Gravity Load - End View; No Symmetry Conditions on Support Pylon

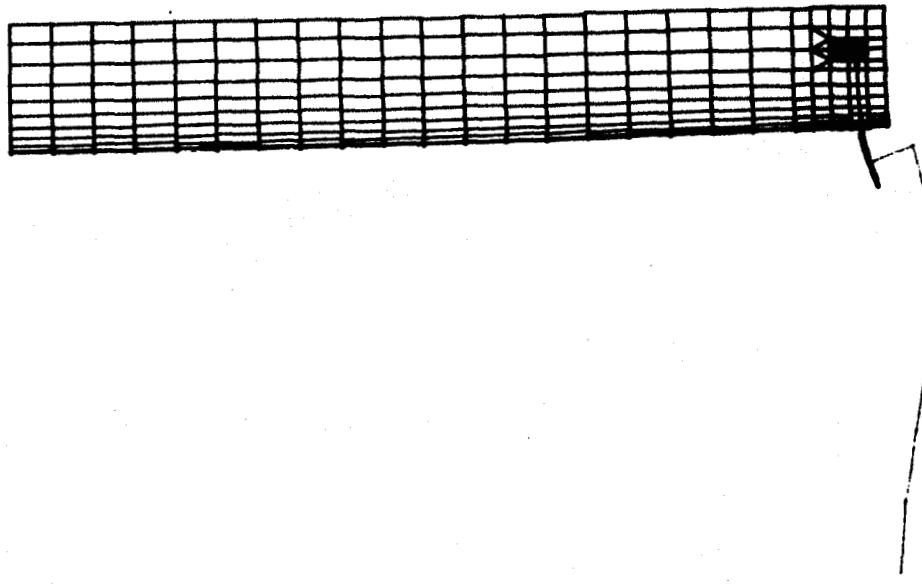

Figure 32. 6.0 m Long Reflector with Support Mecharism under Gravity Load - Side View; No Symmetry Conditions on Support Pylon

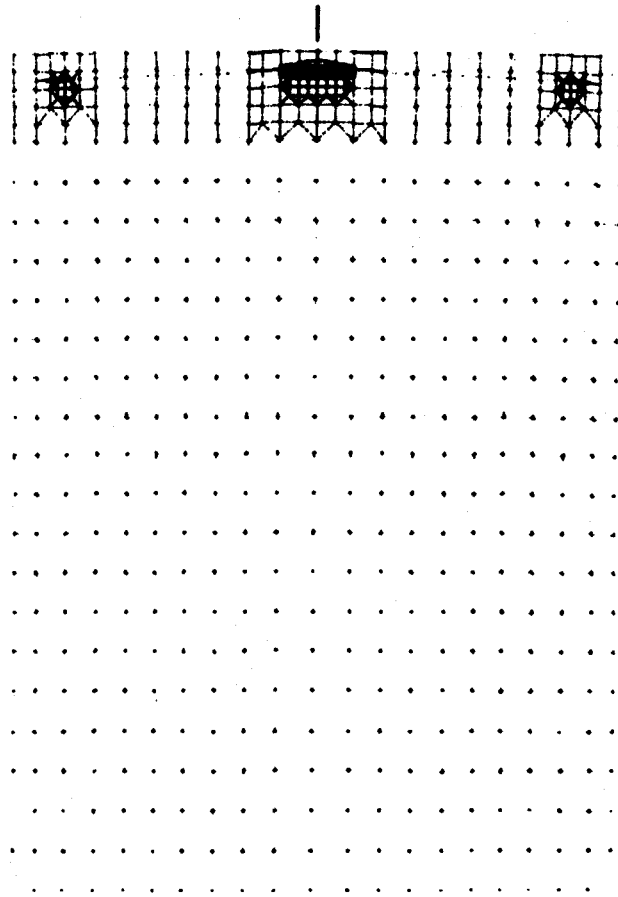

Figure 33. 6.0 m Long Reflector with Support Mechanism under Gravity Load - Top View; No Symmetry Conditions on Support Pylon

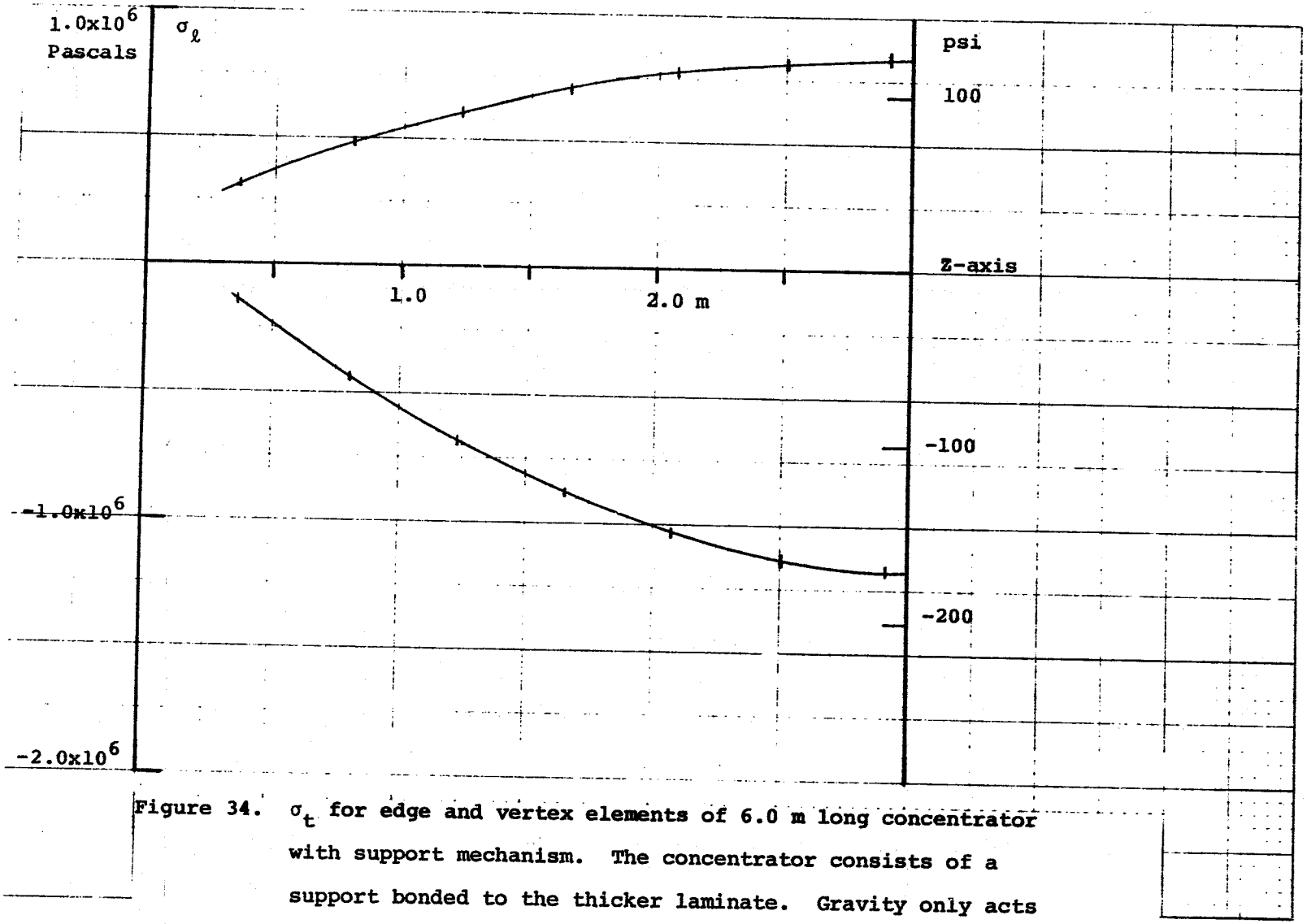

Figure 34. σ_t for edge and vertex elements of 6.0 m long concentrator with support mechanism. The concentrator consists of a support bonded to the thicker laminate. Gravity only acts on the concentrator in the -Y direction. No symmetry conditions are applied to the support pylon.

Figure 25, which is for the case with symmetry conditions on the support pylon. The symmetry conditions on the support pylon make it stiffer and this leads to the lower stresses shown in Figure 25.

For the second loading condition, the concentrator is rotated so that it points in the +X direction. Gravity acts in the -Y direction and there are wind loads in the -X direction. The wind loads correspond to a 13.41 mps (thirty mph) wind in one case and a 40.23 mps(ninety mph) wind in another case. Symmetry conditions are imposed on the support pylon.

The deflections for the case with a 13.41 mps (thirty mph) wind are shown in Figures 35 through 37. Stress plots are shown in Figures 38 through 41. As in the previous studies, the values for σ_t are larger than those for σ_ℓ in the region of the attachment points. Figures 38 and 39 show cross-section plots of σ_t near the attachment points. The concentration decays rapidly as the distance from the attachment point increases. Figures 40 and 41 show σ_ℓ at two cross-sections - one near the attachment area and the other at the center. Both of these curves show a number of reverses in curvature along the cross-section. This complex behavior arises from the interaction of the wind and gravity loads, which are of the same order of magnitude. The gravity load causes the top of the concentrator to rotate forward. The wind load opposes this motion somewhat by trying to make

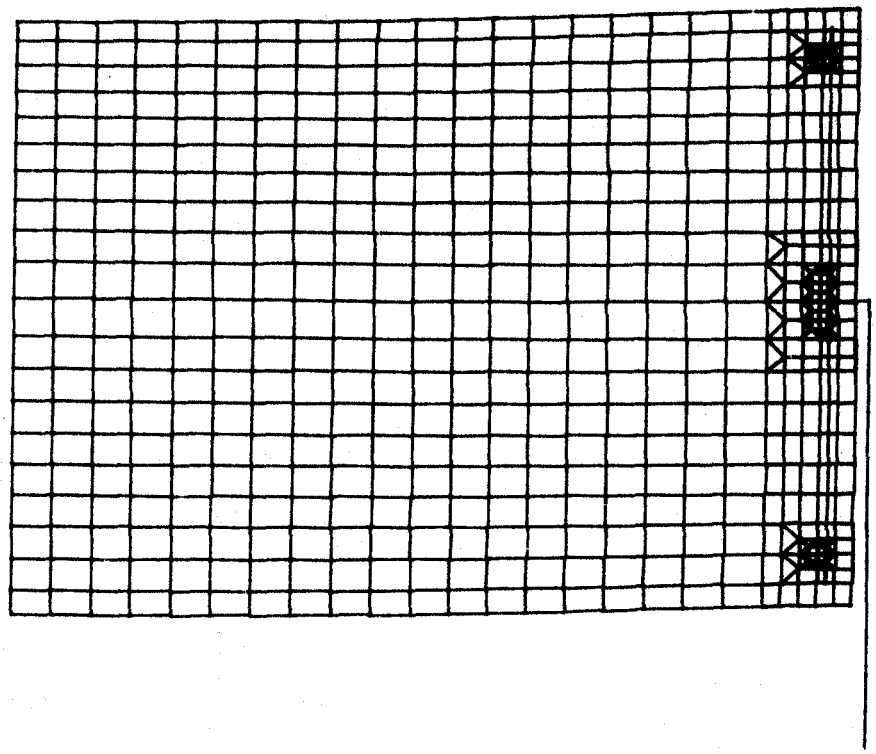

Figure 35. 6.0 m Long Reflector with Support Mechanism under Combined Wind (13.41 mps) and Gravity Loads - Side View; Symmetry Conditions on Support Pylon

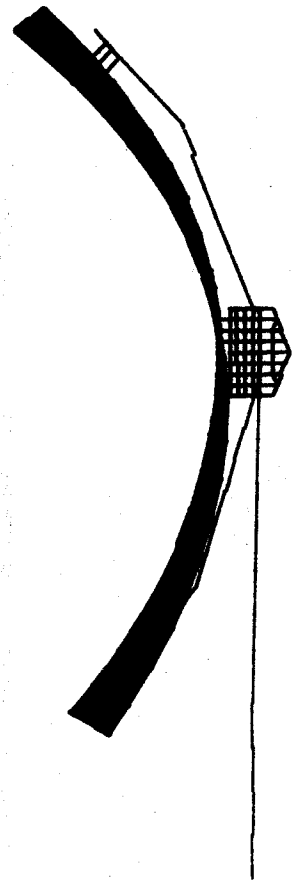

Figure 36. 6.0 m Long Reflector with Support Mechanism under Combined Wind (13.41 mps) and Gravity Loads - End View; Symmetry Conditions on Support Pylon

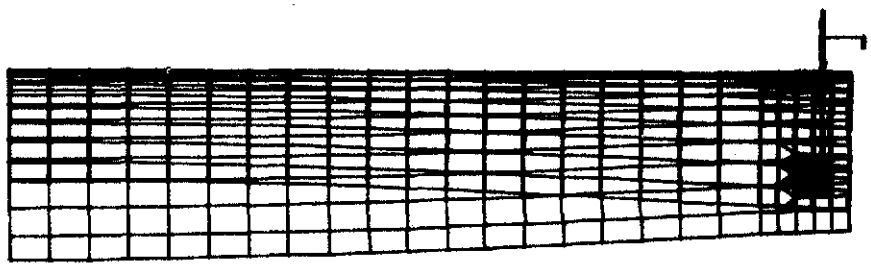

Figure 37. 6.0 m Long Reflector with Support Mechanism under Combined Wind (13.41 mps) and Gravity Loads - Top View; Symmetry Conditions on Support Pylon

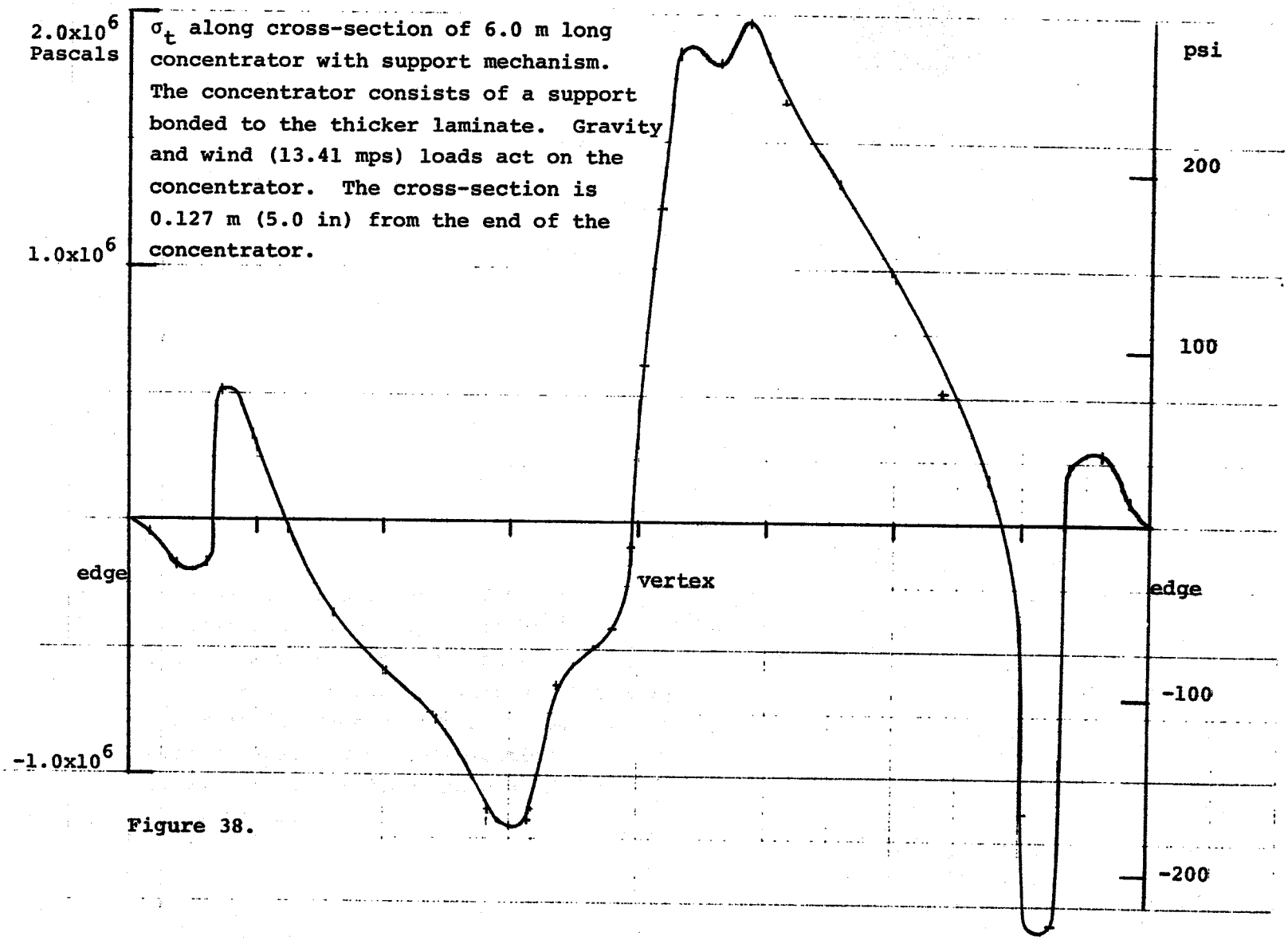

σ_t along cross-section of 6.0 m long concentrator with support mechanism. The concentrator consists of a support bonded to the thicker laminate. Gravity and wind (13.41 mps) loads act on the concentrator. The cross-section is 0.127 m (5.0 in) from the end of the concentrator.

Figure 38.

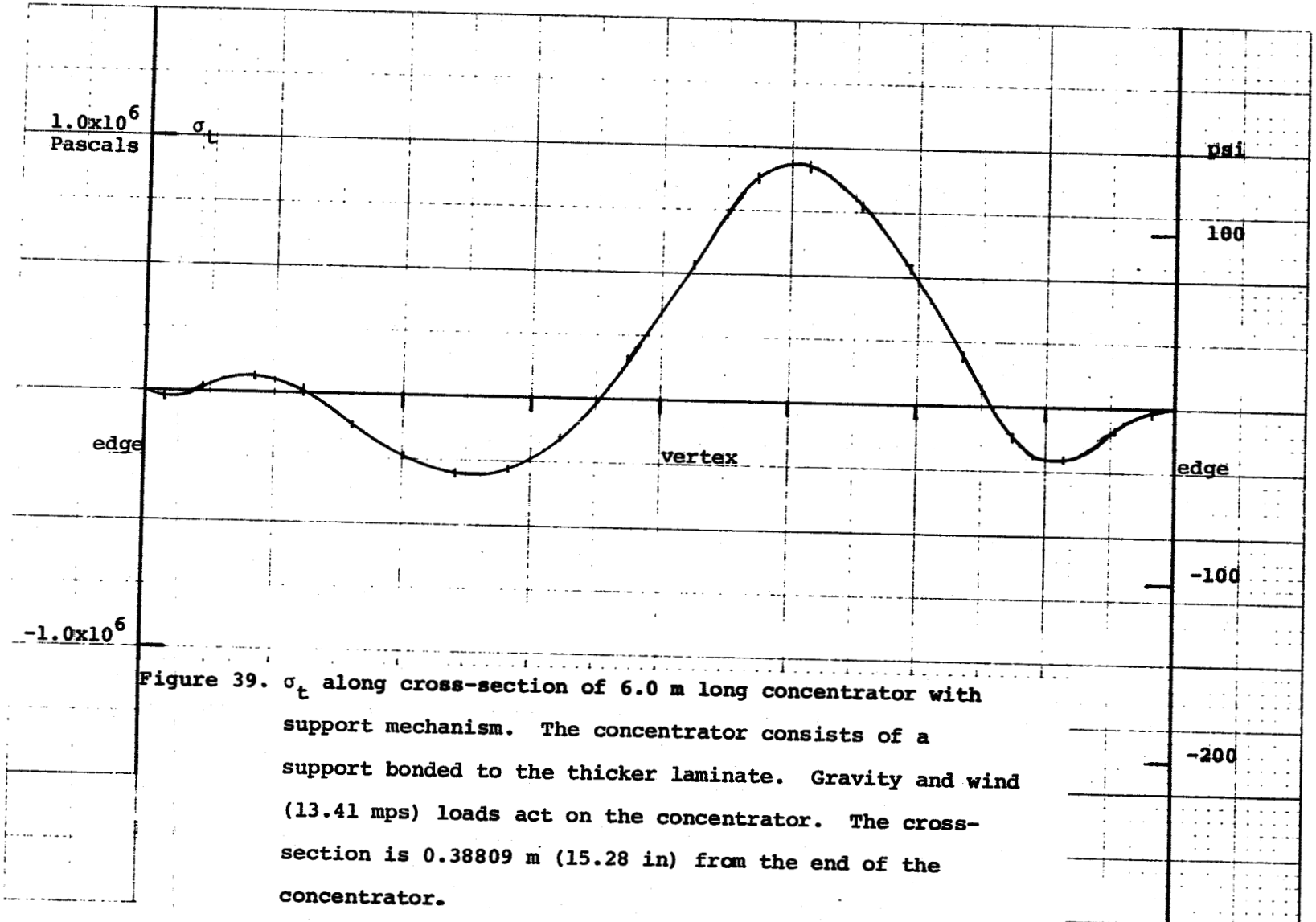

Figure 39. σ_t along cross-section of 6.0 m long concentrator with support mechanism. The concentrator consists of a support bonded to the thicker laminate. Gravity and wind (13.41 mps) loads act on the concentrator. The cross-section is 0.38809 m (15.28 in) from the end of the concentrator.

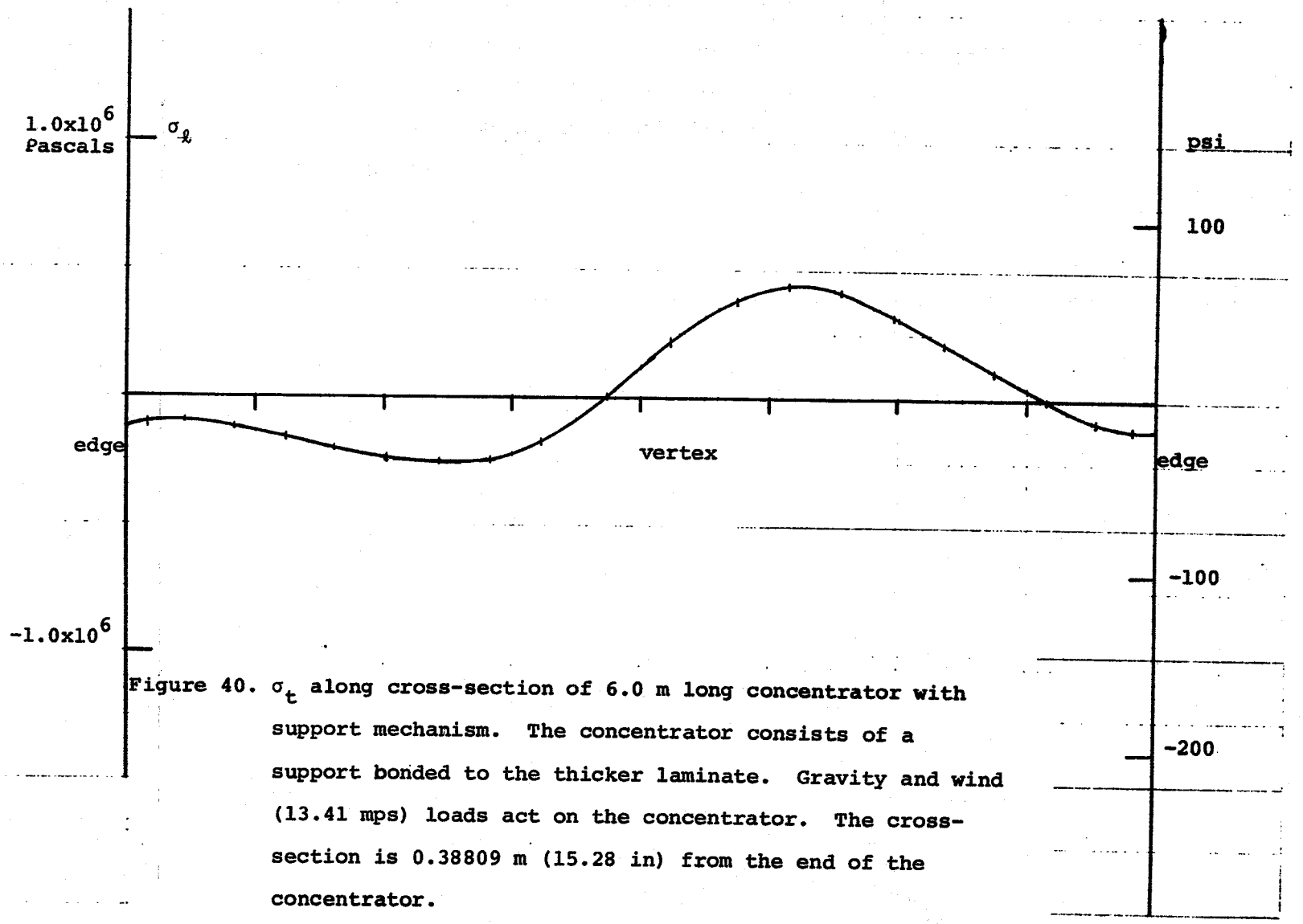

Figure 40. σ_t along cross-section of 6.0 m long concentrator with support mechanism. The concentrator consists of a support bonded to the thicker laminate. Gravity and wind (13.41 mps) loads act on the concentrator. The cross-section is 0.38809 m (15.28 in) from the end of the concentrator.

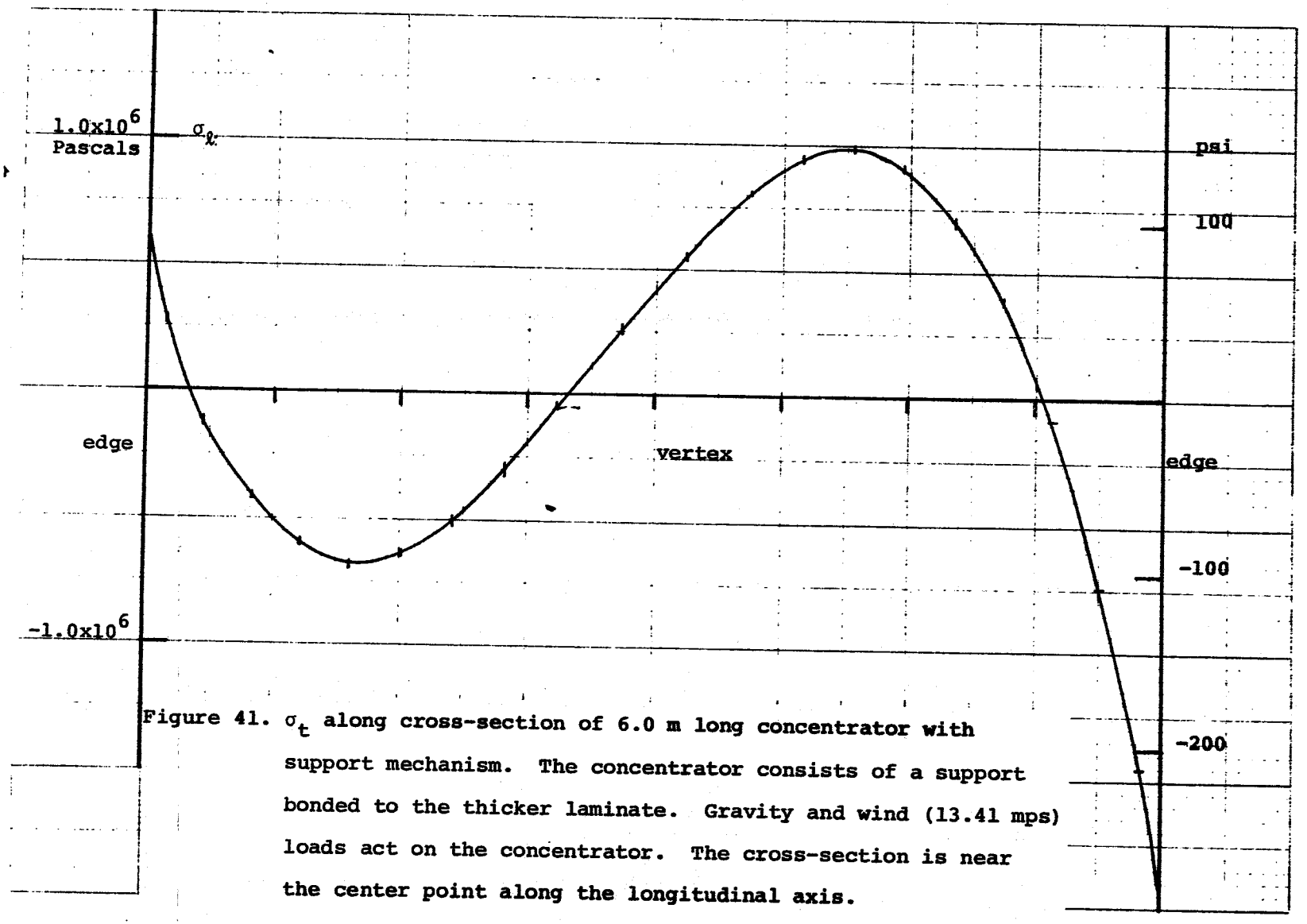

Figure 41. σ_t along cross-section of 6.0 m long concentrator with support mechanism. The concentrator consists of a support bonded to the thicker laminate. Gravity and wind (13.41 mps) loads act on the concentrator. The cross-section is near the center point along the longitudinal axis.

the concentrator "open up." The interaction of these two loads is reflected in the complex curves for the stress σ_ℓ.

The deflections for the case with a 40.23 mps (ninety mph) wind are shown in Figures 42 through 44. A plot of σ_t near the attachment points is shown in Figure 45. For this particular case, the wind loads are beginning to dominate the gravity loads. With wind acting alone, the plot for σ_t would be symmetric about the vertex. Gravity effects introduce asymmetry into the plot. Figure 46 shows a cross-section plot for σ_ℓ at the center of the concentrator. As in the previous plot, the dominance of the wind loads shows up by the fact that the curve is nearly symmetric about the vertex.

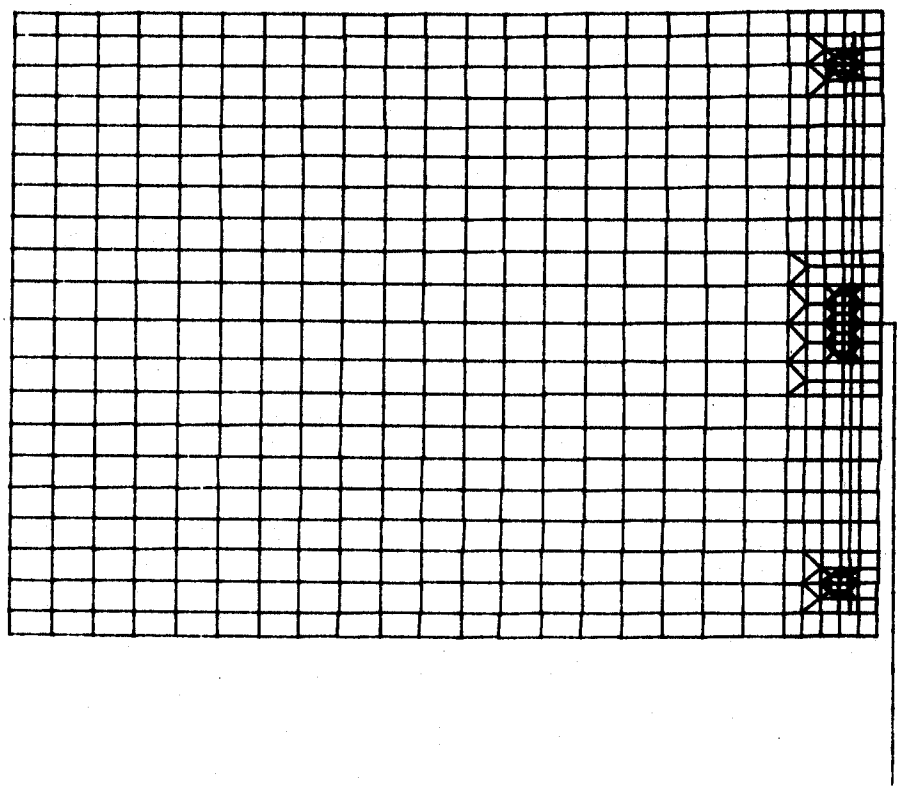

Figure 42. 6.0 m Long Reflector with Support Mechanism under Combined Wind (144 kph) and Gravity Loads - Side View; Symmetry Conditions on Support Pylon

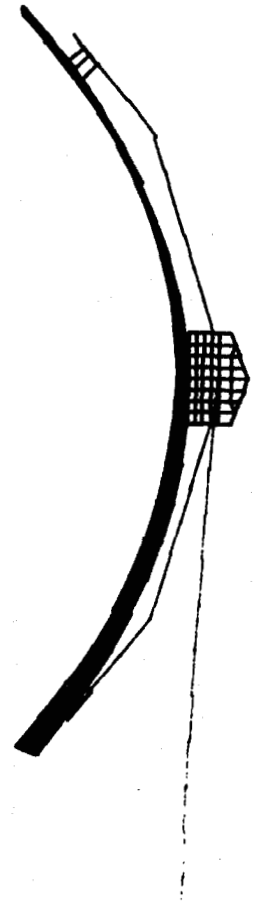

Figure 43. 6.0 m Long Reflector with Support Mechanism under Combined Wind (144 kph) and Gravity Loads - End View; Symmetry Conditions on Support Pylon

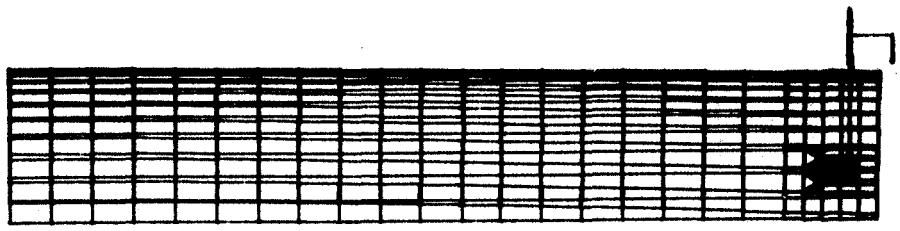

Figure 44. 6.0 m Long Reflector with Support Mechanism under Combined Wind (144 kph) and Gravity Loads - Top View; Symmetry Conditions on Support Pylon

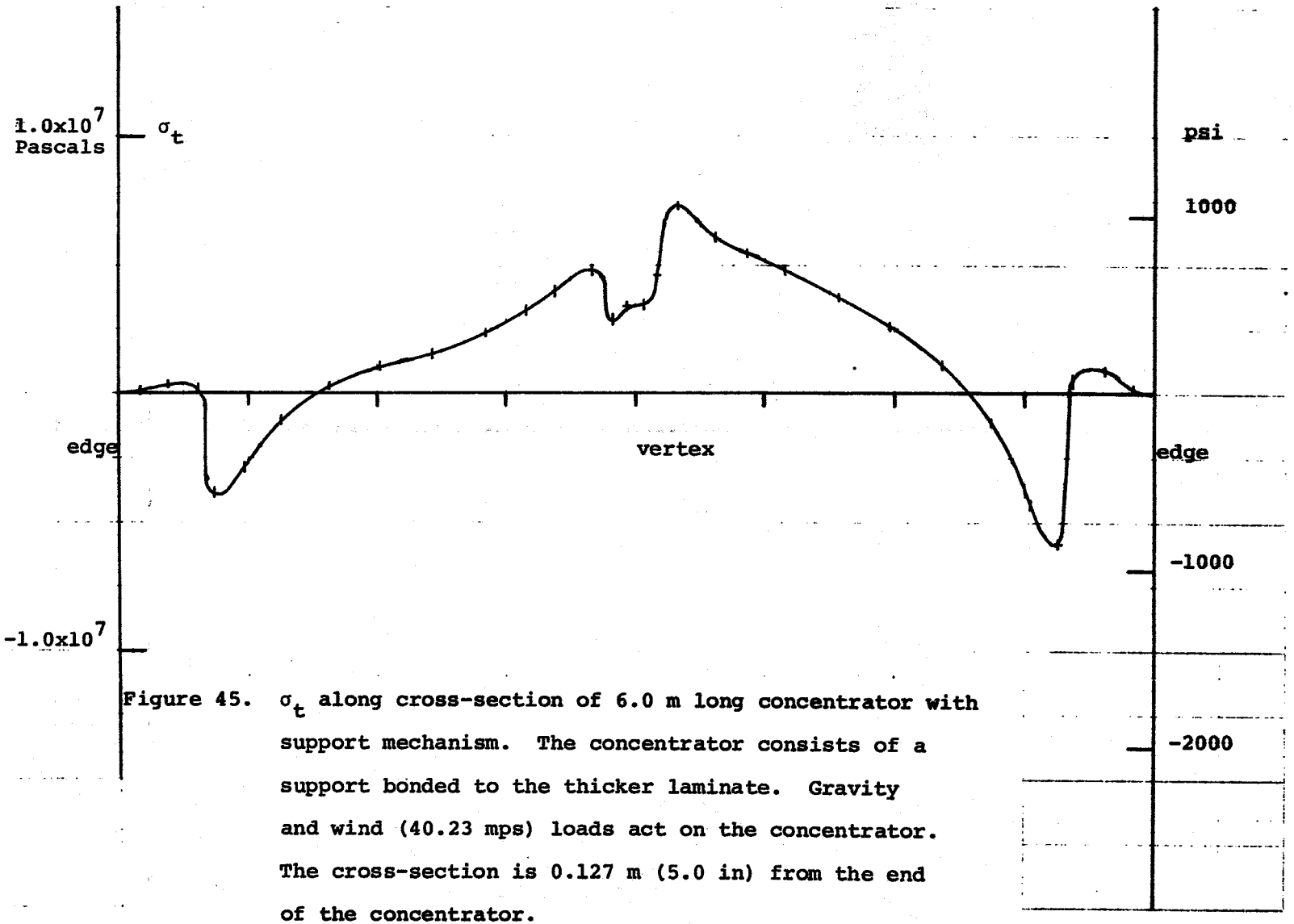

Figure 45. σ_t along cross-section of 6.0 m long concentrator with support mechanism. The concentrator consists of a support bonded to the thicker laminate. Gravity and wind (40.23 mps) loads act on the concentrator. The cross-section is 0.127 m (5.0 in) from the end of the concentrator.

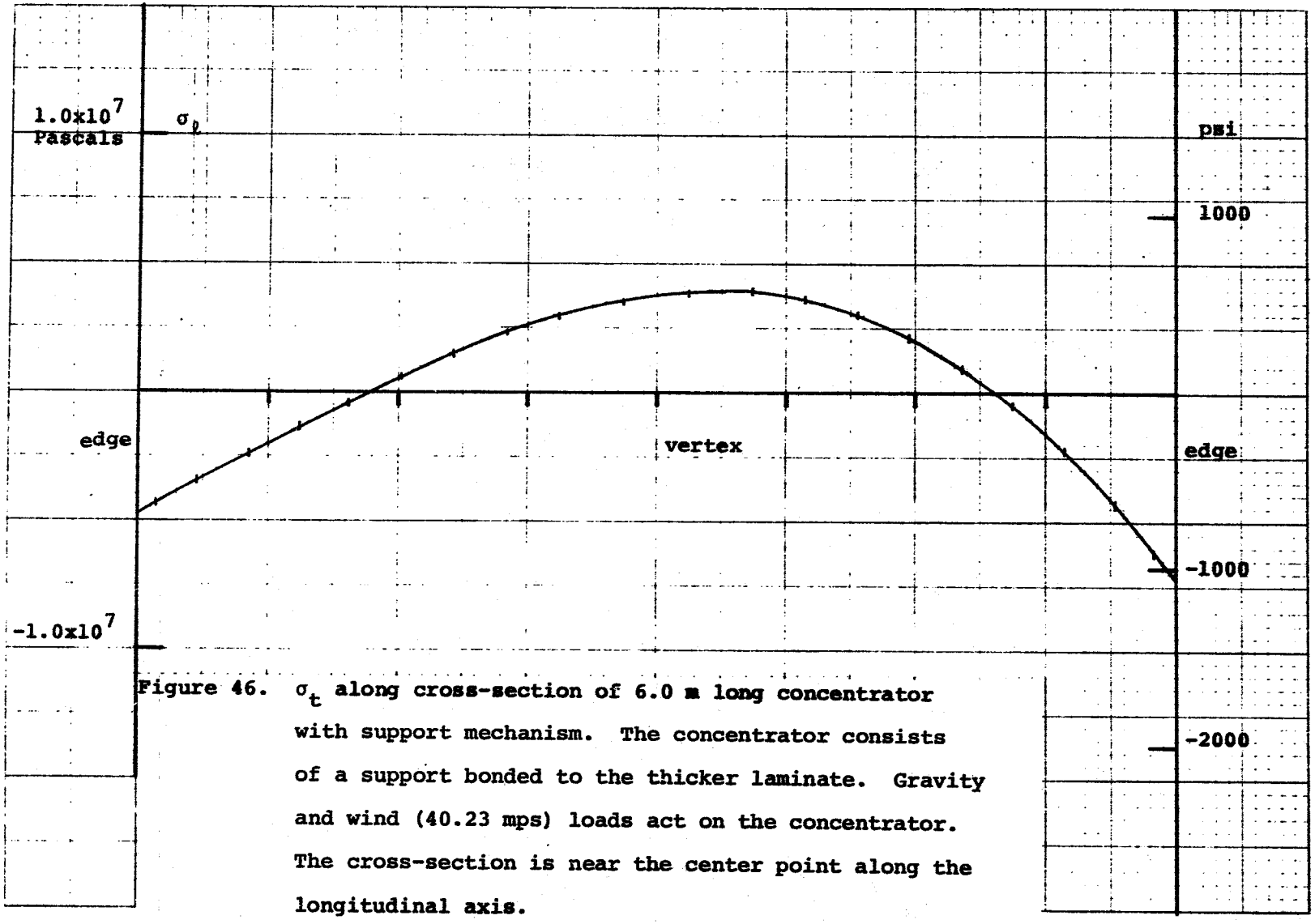

Figure 46. σ_t along cross-section of 6.0 m long concentrator with support mechanism. The concentrator consists of a support bonded to the thicker laminate. Gravity and wind (40.23 mps) loads act on the concentrator. The cross-section is near the center point along the longitudinal axis.

CONCLUSIONS

From the studies which have been made, a 6.0 m (twenty ft.) long parabolic trough solar concentrator appears to be capable of meeting performance and survivability criteria. The concentrator consists of a reflector laminate (made of 0.508 mm (0.02 in.) thick glass and 1.016 mm (0.01 in.) thick steel backing) bonded to an aluminum honeycomb support (made of 0.0254 m (1.0 in.) thick honeycomb aluminum core with 0.508 mm (0.02 in.) thick steel skins). A 6.0 m concentrator consisting of a thinner reflector laminate (made of 0.254 mm (0.01 in.) thick glass and 0.508 mm (0.02 in.) thick steel backing) also appears to be able to meet survivability and performance criteria. The thinner laminate has thirty per cent higher stresses than the thicker laminate.

Computer models which utilize the combined rigidity of the reflector laminate and aluminum honeycomb support structure indicate that a 7.5 m (twenty-four ft.) long concentrator made with the thicker laminate is capable of meeting the restriction that Δ/R_1 be less than or equal to 6.0 milliradians in a 13.41 mps (thirty mph) wind. The value for Δ/R_1 for the 7.5 m long concentrator does not exceed 3.0 milliradians in a combined wind (13.41 mps) and gravity load. This is with the concentrator oriented at a forty-five degree angle to the wind. The values for Δ/R_1 are, of course, smaller for the 6.0 m

concentrator for the same loading configuration.

Although the 7.5 m concentrator does meet the performance criterion in a 13.41 mps wind, the stresses in the glass become too large in a 40.23 mps (ninety mph) wind. Hence, the survivability criterion is not met. The 6.0 m concentrator meets the optical performance in a 13.41 mps wind, and the glass stresses are within acceptable limits in a 40.23 mps wind for those cases studied. For the loadings considered, the largest stresses for a combined wind and gravity load on a concentrator-support mechanism arise at the center of the concentrator and at the points where the concentrator attaches to the support mechanism. For the case of a 40.23 mps wind loading with the concentrator pointing in a horizontal direction and the wind blowing into the concave side, the maximum tensile stress in the glass is near the attachment points and has a value of 7.0 MPa ($\sim$1000 psi). If the wind is reversed, the maximum tensile stress in the glass is near the center and has a value of 7.0 MPa ($\sim$1000 psi). All of the stresses just discussed for the glass are from models which utilize the combined stiffness of the reflector laminate and aluminum honeycomb support structure in the concentrator model.

The conclusion that a 6.0 m concentrator would meet performance and survivability criteria was made on a limited number of loading conditions. The loading conditions which were studied were assumed to be some of the more severe. A more complete analysis would examine other loading conditions to confirm this assumption.

Bibliography

1. NASTRAN User's Guide: Level 15, NASA Report CR-2504, Prepared by Universal Analytics, Inc., Los Angeles, April 1975.

Appendix A

For multilayer plates, such as that shown in Figure A.1, it is necessary to calculate parameters defining the bending and membrane stiffness of the plate. The bending stiffness, denoted by D, for an n layer plate is given by

$$D = \Sigma_{i=1}^{n} \{\left[1/3(a_i^3 - a_{i-1}^3) - 1/2(a_i^2 z_n - a_{i-1}^2 z_n)\right] E_i/(1 - \nu_i^2)\},$$

where z_n denotes the neutral axis of the section. The neutral axis for a multilayer plate is given by

$$z_n = \left[1/2\ \Sigma_{i=1}^{n}\ (a_i^2 - a_{i-1}^2)E_i\right]/\left[\Sigma_{i=1}^{n}\ E_i(a_i - a_{i-1})\right].$$

For a single layer (homogeneous) plate, the above equations give

$$D = Et^3/\left[12(1-\nu^2)\right]$$

and

$$z_n = t/2,$$

where t is the thickness of the single layer. The membrane stiffness is characterized by

$$K_M = \Sigma_{i=1}^{n} \left[(a_i - a_{i-1}) E_i \right].$$

The construction of two reflector laminate-support combinations is given in Tables A.1 and A.2 along with values for D and K_M. The values for D and K_M are used tc define properties for the plate elements used in the finite element studies.

The channels along the edges and end of the reflector are shown in Figure A.2. The cross-sectional properties used to define the structural characteristics of the channels are given in Figure A.3.

Table A.1.

Properties for Support Bonded to Thin Laminate

Material		Thickness m
Glass	Reflector laminate	.000254
Adhesive		.000127
Steel		.000508
Adhesive		.000254
Steel	Support	.000508
Honeycomb		.0254
Steel		.000508

Properties of Materials in Layers

Material	E	ν	ρ
	Elastic Modulus	Poisson's Ratio	Density
Steel	200.0 GPa	0.30	7850 kg/m^3
	(29.0×10^6 psi)		0.282 lb/in^3
Glass	68.95 GPa	0.24	2297 kg/m^3
	(10.0×10^6 psi)		0.083 lb/in^3
Adhesive	3.4475 GPa	0.37	1661 kg/m^3
	(5.0×10^5 psi)		0.060 lb/in^3
Honeycomb	0.2758 GPa	0.48	
	(4.0×10^4 psi)		

Composite Properties of Laminate Plate

$D = 5.3725 \times 10^4$ Pa - m^3

$K_M = 3.3063 \times 10^8$ Pa - m

$z_n = .018230$ m

Table A.2.

Properties of Support Bonded to Thick Laminate

Material		Thickness m
Glass	Reflector Laminate	.000508
Adhesive		.000127
Steel		.001016
Adhesive		.000254
Steel	Support	.000508
Honeycomb		.0254
Steel		.000508

Properties of Materials in Layers

Material	E	ν	ρ
	Elastic Modulus	Poisson's Ratio	Density
Steel	200.0 GPa	0.30	7850 kg/m^3
	(29.0 x 10^6 psi)		0.282 lb/in^3
Glass	68.95 GPa	0.24	2297 kg/m^3
	(10.0 x 10^6 psi)		0.083 lb/in^3
Adhesive	3.4475 GPa	0.37	1661 kg/m^3
	(5.0 x 10^6 psi)		0.060 lb/in^3
Honeycomb	0.2758 GPa	0.48	
	(4.0 x 10^4 psi)		

Composite Properties of Laminate Plates

$D = 6.2068 \times 10^4$ Pa - m^3

$K_M = 4.4975 \times 10^8$ Pa - m

$z_n = .02072$ m

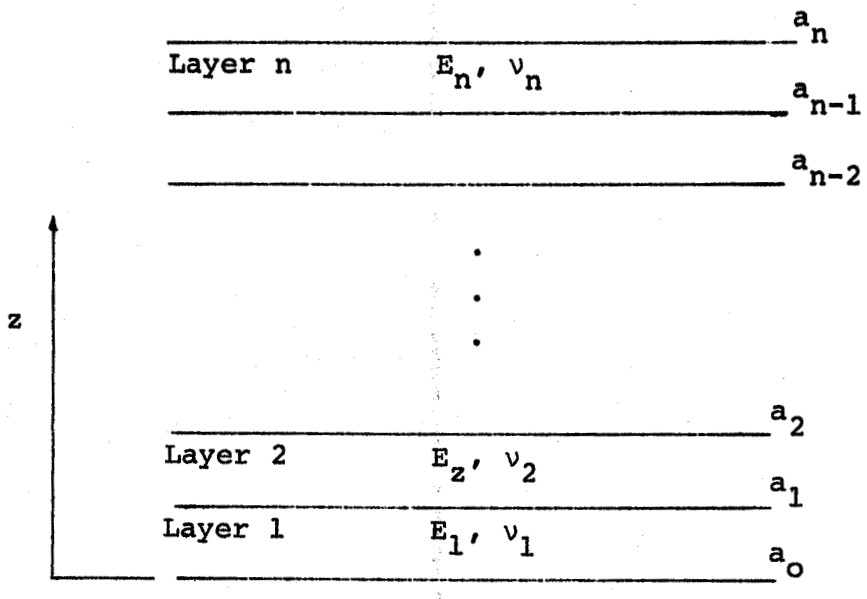

Figure A.1. Notation for Multilayer Plate

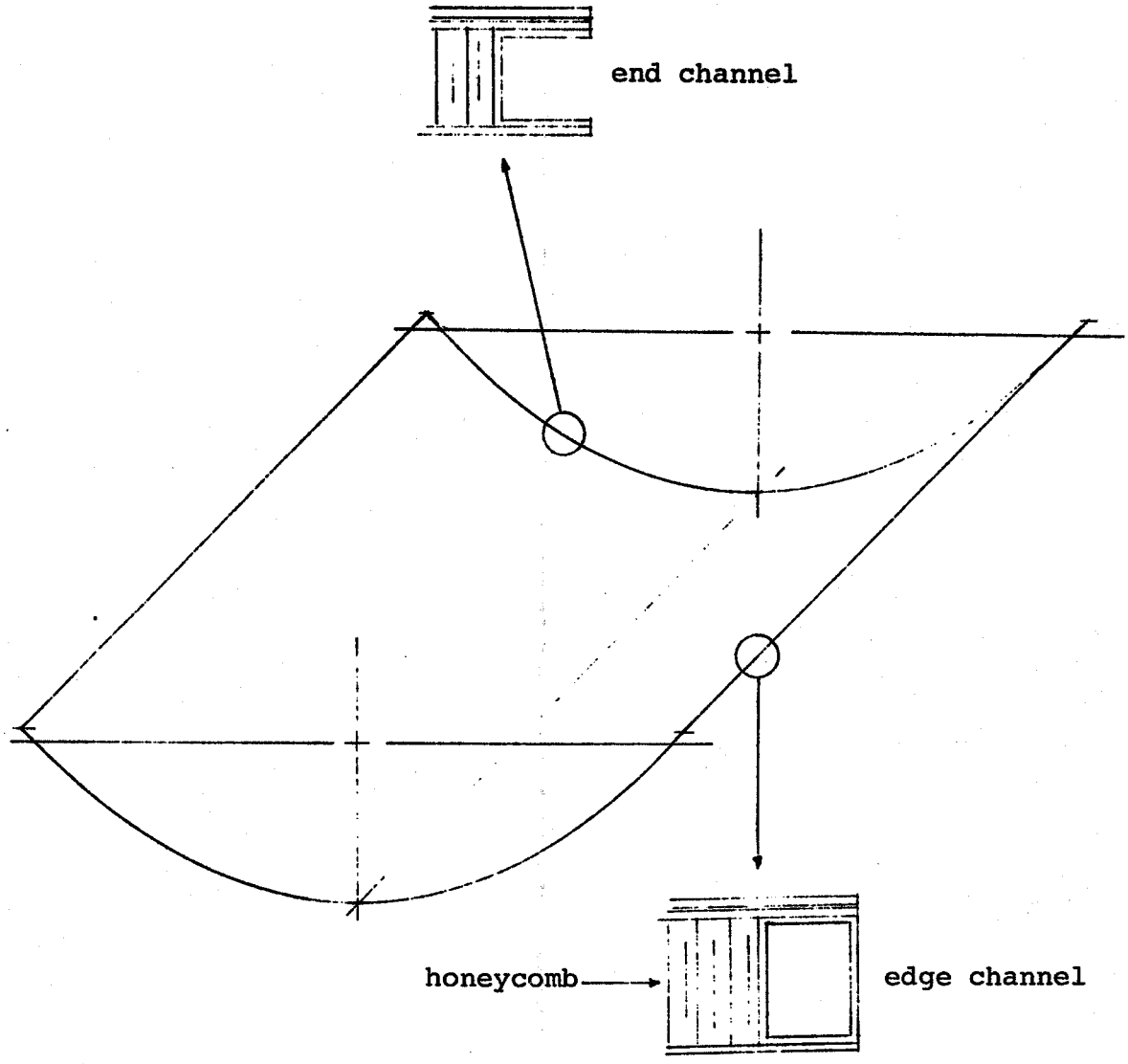

Figure A.2. Edge and End Channels for Concentrator

Edge Channel

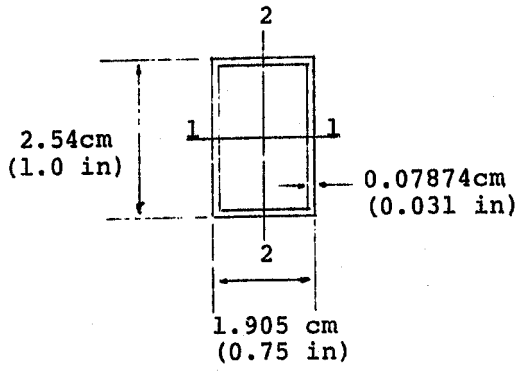

$A = 6.752 \times 10^{-5}\ m^2$

$I_1 = 6.3197 \times 10^{-9}\ m^4$

$I_2 = 4.0376 \times 10^{-9}\ m^4$

$J = 7.1580 \times 10^{-9}\ m^4$

End Channel

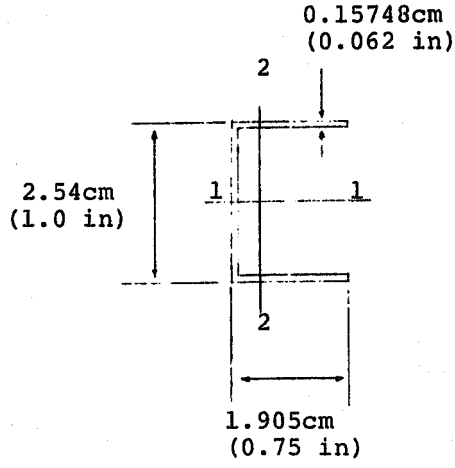

$A = 9.5040 \times 10^{-5}\ m^2$

$I_1 = 9.9726 \times 10^{-9}\ m^4$

$I_2 = 3.5083 \times 10^{-9}\ m^4$

$J = 8.0616 \times 10^{-11}\ m^4$

A = area of cross section

I_1 = area moment of inertia about 1 axis

I_2 = area moment of inertia about 2 axis

J = polar moment of inertia

Figure A.3. Section Properties for Edge and End Channels for Concentrator.

Appendix B

The mesh used for the finite element model of the concentrator-support mechanism combination is shown in Figures B.1 through B.3. The support consists of a pedestal which is topped by a portion of the drive mechanism. Both of these components of the support are modeled with beam elements. The drive mechanism is attached to a plate, which is also attached to two ribs. The plate and ribs are attached to the concentrator at four different locations. The plate is modeled with plate elements and the ribs are modeled with beam elements.

Aluminum plates (doublers) 0.01524 mm (0.06 in.) thick are added to the honeycomb support at the attachment points. The equivalent properties of some of the plates elements in the concentrator are specified so that the bending and membrane stiffness of the doubler-honeycomb-laminate combination are correctly modeled. The elements are indicated in Figure B.4.

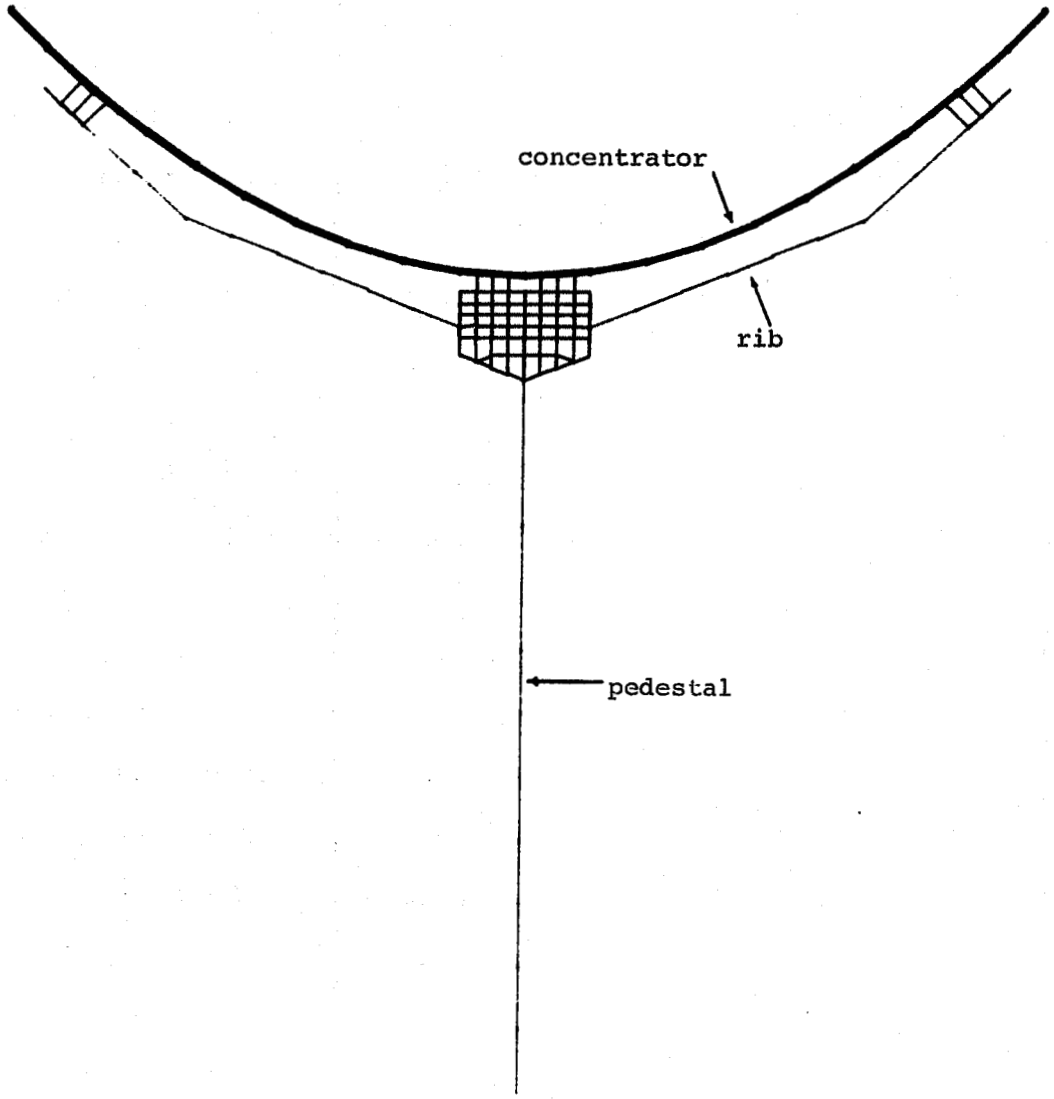

Figure B.1. End View of Concentrator - Support Mechanism Combination.

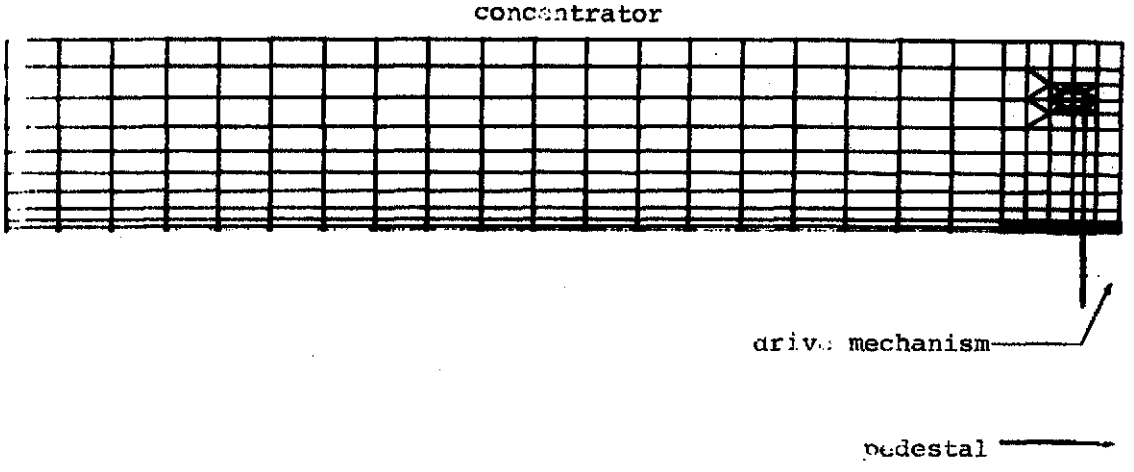

Figure B.2. Side View of Concentrator - Support Mechanism Combination.

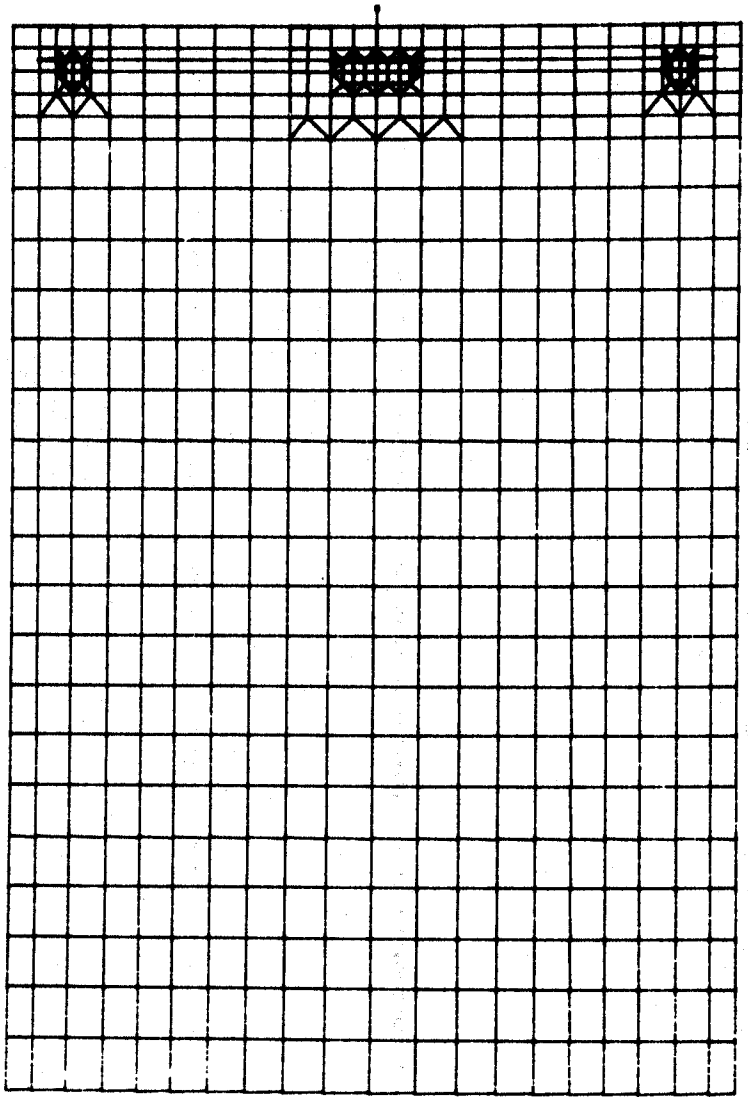

Figure B.3. Top View of Concentrator - Support Mechanism Combination.

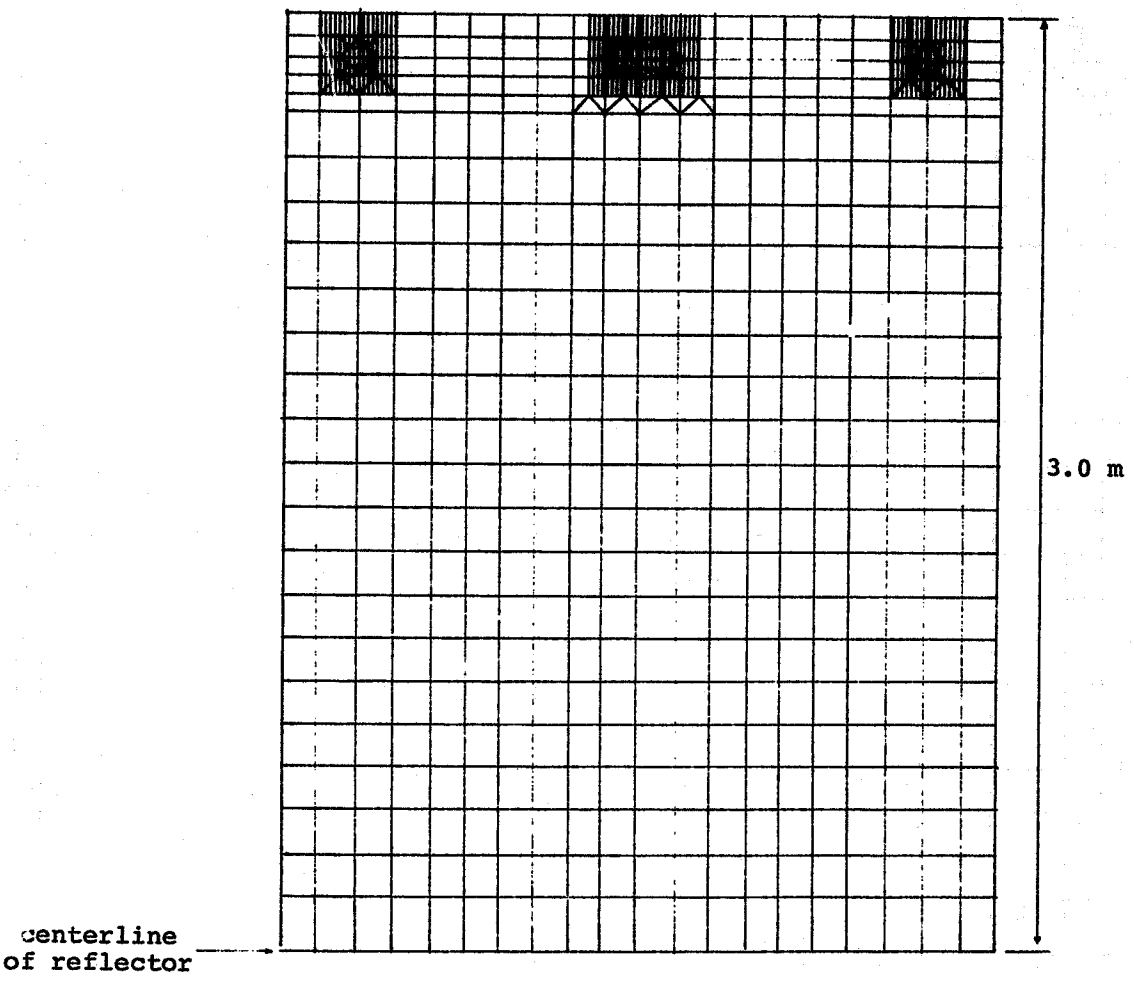

Figure B.4. Plate Elements with Equivalent Stiffness to Represent Doubler-Honeycomb-Laminate Construction (Indicated by Shaded Areas).

Distribution:

J. Vidum
Acurex Corporation
485 Clyde Avenue
Mountain View, CA 94042

G. Hutchinson
Solar Kinetics, Inc.
8120 Chancellor Row
Dallas, TX 75247

V. Reese
Suntec Systems, Inc.
2101 Wooddale Drive
St. Paul, MN 55119

M. Delgado
Del Manufacturing Co.
905 Monterey Pass Road
Monterey Park, CA 91754

J. R. Schuster
General Atomic Company
P. O. Box 81608
San Diego, CA 92138

G. Branch
Hexcel Corporation
11711 Dublin Blvd
Dublin, CA 94566

A. Stocker
Harrison Radiator Division
General Motors
Lockport, NY

J. F. Britt
Technical Center
General Motors Corp.
Warren, MI 48090

J. Hamilton
Exxon Enterprises
P. O. Box 592
Florham Park, NJ 07923

W. W. Dickhart
Budd Company
Fort Washington, PA 19034

A. F. Shoemaker
Corning Glass Co.
Corning, N. Y. 14830

J. R. Williams
Energy Resources Center
Honeywell, Inc.
2600 Ridgeway Parkway
Minneapolis, MN 55413

M. Faeth
Highland Plating
1128 N. Highland
Los Angeles, CA 90038

H. J. Sund
Ford Aerospace & Communications
3839 Fabian Way
Palo Alto, CA 94303

P. Bender
Ford Glass Division
300 Renaissance Center
P. O. Box 43343
Detroit, MI 48243

W. J. Nagle
Ford Motor Co.
Room E-3184
Scientific Research Labs
Dearborn, MI 48121

R. C. Frounfelter
PPG Industries, Inc.
1 Gateway Center
Pittsburgh, PA 15222

D. L. Thomas
PPG Industries, Inc.
Glass Research Center
Box 11472
Pittsburgh, PA 15238

R. E. Cook
Donnelly Mirrors, Inc.
49 West Third Street
Holland, MI 49423

C. M. Lemrow
Electrical Products Division
Corning Glass Works
Corning, NY 14830

C. G. Lawson
Union Carbine Corp
P. O. Box X
Oak Ridge, TN 37830

C. M. Lemrow
Electrical Products Division
Corning Glass Works
Corning, NY 14830

M. Mitchel
Jacobs Engineering Co.
251 South Lake Avenue
Pasadena, CA 91101

J. N. Epel
The Budd Company
Plastic R&D Center
356 Executive Drive
Troy, MI 48084

Jerry Flynt
Haveg Industries, Inc.
12837 E. Imperial Highway
Santa Fe Springs, CA 90670

J. Rogan
McDonnell Douglas Astro. Co
5301 Bolsa Avenue
Huntington Beach, CA 92647

Solar Energy Res. Inst. (3)
1536 Cole Blvd
Golden, CO 80401
Attn: B. Gupta
B. L. Butler
M. Cotton

U. S. Dept of Energy (3)
Albuquerque Operations Office
P. O. Box 5400
Albuquerque, NM 87185
Attn: J. Weisiger
D. N. Pappas
W. P. Grace

U. S. Department of Energy
San Francisco Operations Office
1333 Broadway
Oakland, CA 94612
ATTN: W. D. Nettleton

U. S. Department of Energy (8)
Division of Central Solar Tech.
Washington, D. C. 20545
Attn: G. W. Braun
M. U. Gutstein
J. E. Rannels
M. E. Resner

U. S. Department of Energy (2)
Agricultural & Industrial Process
Heat Cons. & Solar Application
Washington, DC 20545
Attn: W. W. Auer
J. Dolland

1472 L. G. Rainhart
1500 W. A. Gardner
1550 F. W. Neilson
1552 O. J. Burchett
1556 S. A. Ingham
2320 K. Gillespie
2323 C. M. Gabriel
2324 R. S. Pinkham
2326 G. M. Heck
3161 J. E. Mitchell
3700 J. C. Strassell
4000 A. Narath
4231 J. H. Renken
4700 J. H. Scott
4710 G. E. Brandvold
4721 V. L. Dugan (5)
4721 J. V. Otts
4722 J. F. Banas (25)
4723 W. P. Schimmel
4725 J. A. Leonard
5500 O. E. Jones
5510 D. B. Hayes
5520 T. B. Lane
5523 R. C. Reuter, Jr.
5523 J. R. Koteras
5530 W. Herrmann
5810 R. G. Kepler
5811 L. A. Harrah
5813 J. G. Curro
3141 T. L. Werner (5)
3151 W. L. Garner (3)
3154-4 R. P. Campbell (25)
for DOE/TIC